LASER INTERFEROMETER GRAVITATIONAL WAVE OBSERVATORY
- LIGO -
CALIFORNIA INSTITUTE OF TECHNOLOGY
MASSACHUSETTS INSTITUTE OF TECHNOLOGY

Technical Note	**LIGO-TT1700104-v2**	2017/03/17

aLIGO, SQZ, VOPO Cavity, Final Optical Design

J. Miller, L. Barsotti, F. Matichard, M. Evans, A. Fernández and P. Fritschel

Distribution of this document:

LIGO LAB

California Institute of Technology
LIGO Project, MS 18-34
Pasadena, CA 91125
Phone (626) 395-2129
Fax (626) 304-9834
E-mail: info@ligo.caltech.edu

Massachusetts Institute of Technology
LIGO Project, Room NW17-161
Cambridge, MA 02139
Phone (617) 253-4824
Fax (617) 253-7014
E-mail: info@ligo.mit.edu

LIGO Hanford Observatory
Route 10, Mile Marker 2
Richland, WA 99352
Phone (509) 372-8106
Fax (509) 372-8137
E-mail: info@ligo.caltech.edu

LIGO Livingston Observatory
19100 LIGO Lane
Livingston, LA 70754
Phone (225) 686-3100
Fax (225) 686-7189
E-mail: info@ligo.caltech.edu

http://www.ligo.caltech.edu/

Executive summary

We present the design of the in-vacuum optical parametrical oscillator (VOPO) to be used in aLIGO squeezing experiments.

Contents

1 Overview

The VOPO cavity generates squeezed light which can be used to reduce quantum noise in the interferometer. The cavity is simultaneously resonant at 1064 nm and 532 nm and contains a nonlinear PPKTP crystal housed in a temperature-controlled oven. The geometry of the cavity is chosen such that a small ∼25 µm waist is formed at the mid point of the crystal. The 532 nm field, injected through M1 heading toward M2 (see Fig. 3), acts as an energy source or pump for the nonlinear process. A frequency-shifted 1064 nm beam enters the cavity through M2 heading toward M3. This beam is used in the squeezing control scheme. Important cavity parameters are losses, which limit the achievable level of squeezing, and length noise, which leads to unwanted rotation of the squeezed quadrature.

2 Optical parameters

The optical parameters of the VOPO are listed in Table 1. The transverse mode spectra for 532 nm and 1064 nm are shown in Figure 13. Beam spot sizes as a function of position are presented in Fig. 14. Equivalent plots for the case in which the PPKTP crystal is removed may be found in Appendix C.

Relative to the H1 OPO, we have doubled the green finesse. This reduces the green power which must arrive to the cavity to achieve a given level of squeezing by a factor of two – a potentially beneficial change given our switch to a fibre-based delivery system. It also provides additional filtering of PDH sidebands on the green light (which lead to phase noise). Sensitivity to drifts in dc power is increased but, due to servo control, we do not expect such drifts to occur.

We have also modified the cavity geometry to increase the waist sizes slightly. This may help in mitigating thermal effects and increasing the longevity of the crystal. Any impact on OPO performance should be minor (see §F).

The cavity is stable both with and without the crystal present, allowing estimates of the losses arising due to the crystal to be made.

Table 1: Parameters of the VOPO cavity. Sagittal and tangential planes are denoted by (s) and (t) respectively. The calculation of alignment sensitivity is described in section G.4.

Parameter	532 nm	1064 nm
Finesse, crystal in	34.8	46.1
Linewidth, crystal in	24.499 MHz	18.495 MHz
FSR, crystal in	851.934 MHz	853.452 MHz
ω_0^{small}, crystal in	21.1 µm (s)/21.1 µm (t)	30.0 µm (s)/29.9 µm (t)
ω_0^{large}, crystal in	159.2 µm (s)/148.8 µm (t)	221.2 µm (s)/206.9 µm (t)
g factor, crystal in	0.377 (s)/ 0.444 (t)	0.394 (s)/ 0.460 (t)
Gouy phase, crystal in	0.710π (s)/0.732π (t)	0.716π (s)/0.737π (t)
Alignment sensitivity, crystal in	0.269 m/rad (s)/ 0.303 m/rad (t)	0.277 m/rad (s)/ 0.313 m/rad (t)
Relative alignment sensitivity, crystal in	1.693 ω_0^{large}/mrad (s)/ 2.039 ω_0^{large}/mrad (t)	1.252 ω_0^{large}/mrad (s)/ 1.512 ω_0^{large}/mrad (t)
Offset sensitivity, crystal in	5.389 m/m (s)/ 6.106 m/m (t)	5.539 m/m (s)/ 6.297 m/m (t)
Relative offset sensitivity, crystal in	33.856 ω_0^{large}/mm (s)/ 41.039 ω_0^{large}/mm (t)	25.040 ω_0^{large}/mm (s)/ 30.433 ω_0^{large}/mm (t)
FSR, crystal out	875.282 MHz	
ω_0^{small}, crystal out	18.5 µm (s)/16.2 µm (t)	26.2 µm (s)/22.9 µm (t)
ω_0^{large}, crystal out	94.0 µm (s)/79.9 µm (t)	132.9 µm (s)/113.0 µm (t)
g factor, crystal out	0.833 (s)/ 0.906 (t)	
Gouy phase, crystal out	0.866π (s)/0.901π (t)	
Alignment sensitivity, crystal out	1.021 m/rad (s)/1.812 m/rad (t)	
Relative alignment sensitivity, crystal out	10.864 ω_0^{large}/mrad (s)/ 22.679 ω_0^{large}/mrad (t)	7.682 ω_0^{large}/mrad (s)/ 16.037 ω_0^{large}/mrad (t)
Offset sensitivity, crystal out	20.414 m/m (s)/36.452 m/m (t)	
Relative offset sensitivity, crystal out	217.278 ω_0^{large}/mm (s)/ 456.155 ω_0^{large}/mm (t)	153.639 ω_0^{large}/mm (s)/ 322.550 ω_0^{large}/mm (t)

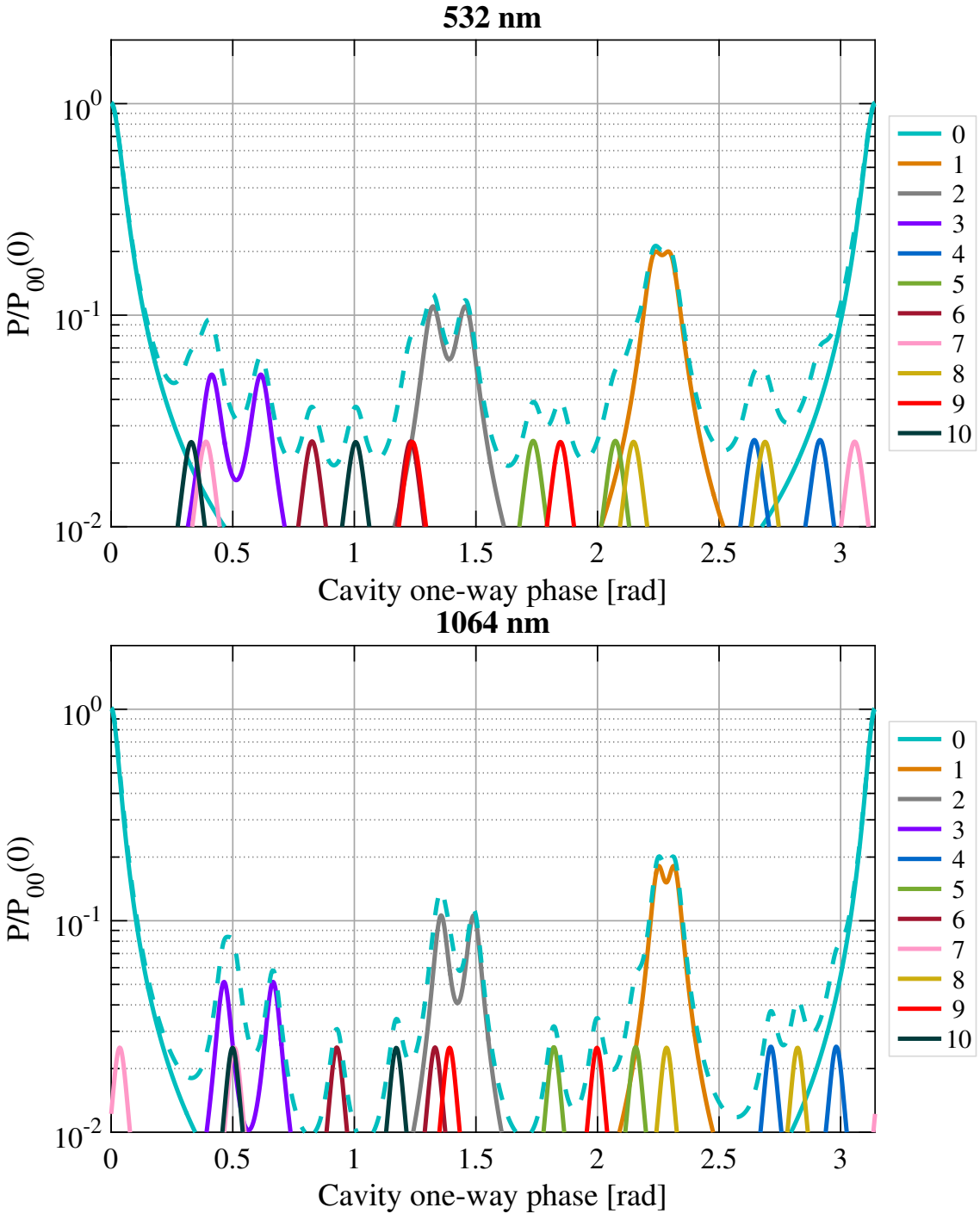

Figure 1: Simulated transverse mode spectrum of the VOPO cavity. Legend values indicate mode order. For each order, peaks are only drawn for the highest and lowest frequency modes (e.g. 20 and 02 but not 11). The relative powers in each mode were chosen arbitrarily. The total power is given by the dashed trace.

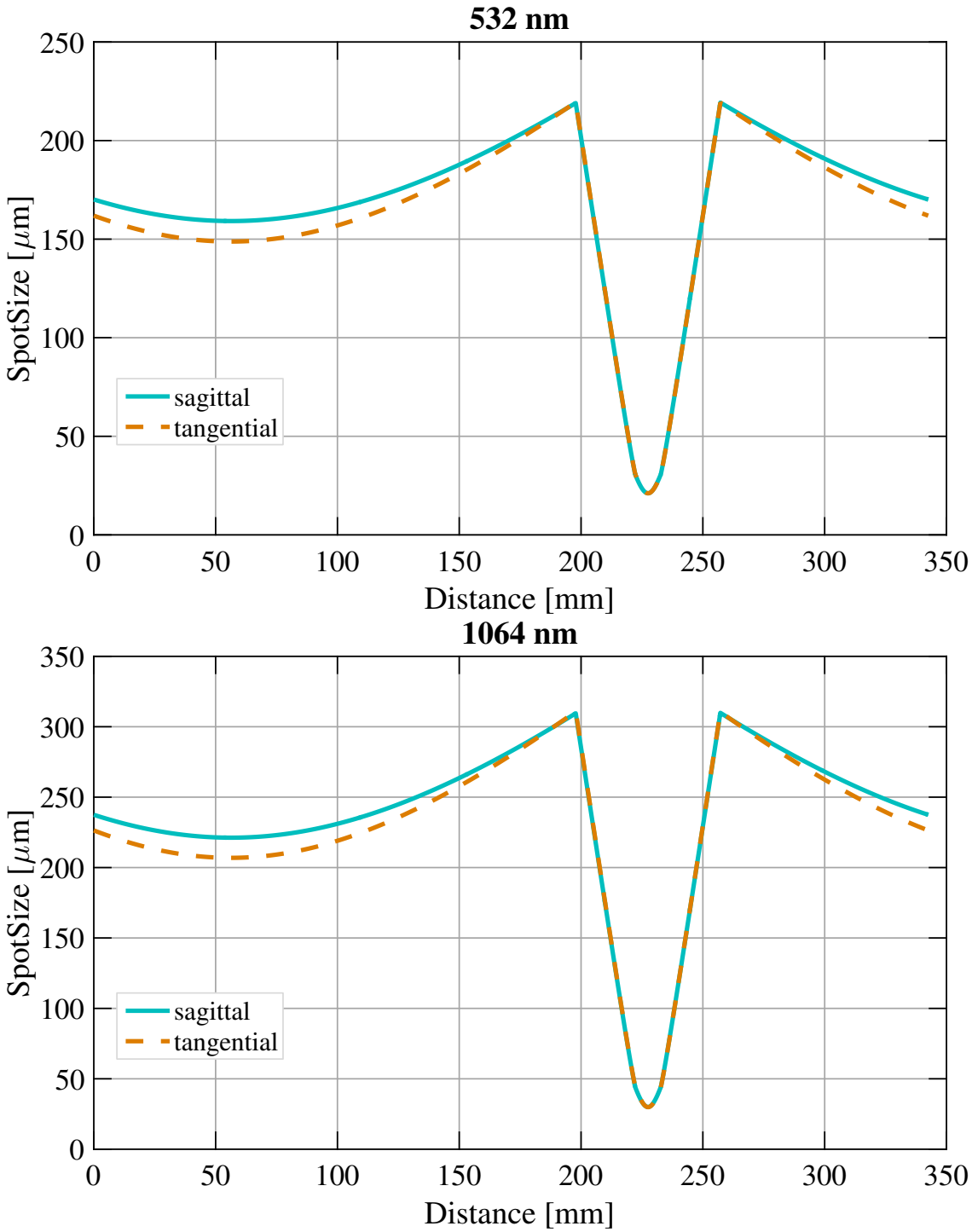

Figure 2: Beam spot size as a function of distance from M1 for the VOPO cavity.

3 Cavity geometry

N.B. After constructing a SOLIDWORKS model, it was found that changing the cavity layout as shown in Figure 3 would eliminate possible interferences between optical components on the VOPO injection platform. The change amounts to mirroring the cavity about the vertical direction. This change has not yet been propagated to any other parts of this document. Existing results may easily be reinterpreted where necessary.

Figure 3 illustrates the VOPO cavity's geometry. The cavity is formed in a bow-tie configuration[1] with two flat mirrors and two identical curved mirrors. Mirror separations are selected to give appropriate spot sizes in the nonlinear crystal and to avoid overlaps between the fundamental and higher-order modes. The angles of incidence on the mirrors are chosen considering astigmatism, ease of construction and ability to separate incoming and reflected beams. The mirror positions and orientations are given in Table 2.

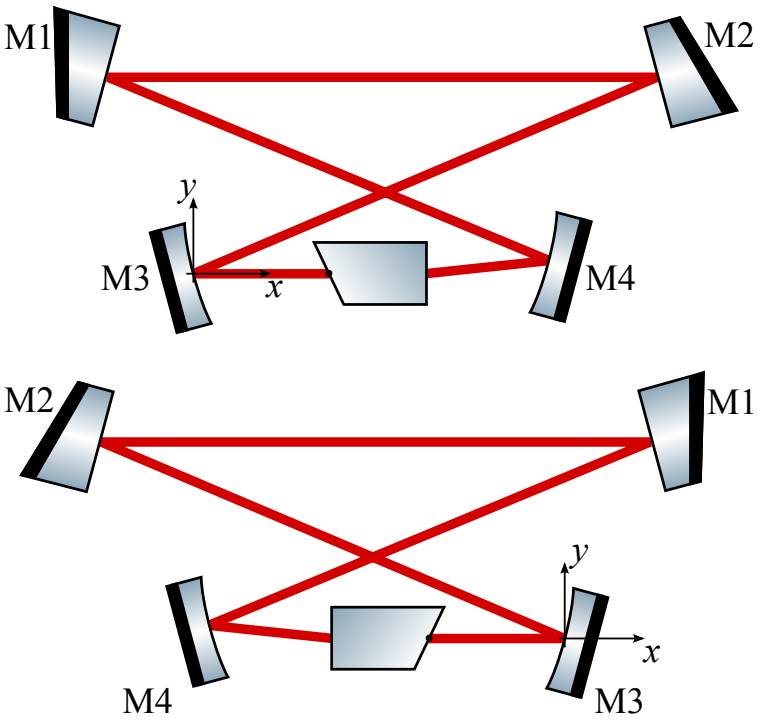

Figure 3: The bow-tie geometry selected for the VOPO cavity (not to scale). Upper - old configuration used in e.g. ray tracing models. Lower - new, as-built, geometry obtained by mirroring about the vertical direction. Wedges should be installed as shown.

This geometry is slightly different to that employed in the H1 experiment. The cavity is slightly larger overall and utilises mirrors with larger radii of curvature. This change yields larger spot sizes, increases robustness against errors in curved mirror separation (the H1 design can become unstable) and more similar g factors with and without the nonlinear

[1] Amongst other beneficial properties, a bow-tie cavity should scatter less light back into the interferometer [1].

Table 2: Positions and orientations of the optics forming the VOPO cavity. Both old and new (as-built, obtained by mirroring about the vertical direction) configurations are presented. The origin of the coordinate system is the centre of the HR surface of M3 (see Fig. 3). The reference point for the PPKTP crystal is the centre of the wedged surface, indicated by a black dot. Angles are measured between the positive x axis and the HR surface normal (dotted surface for PPKTP crystal).*These angles are solely due to the crystal wedge, the crystal is not globally tilted.

	Optic	ROC [mm]	x position [mm]	y position [mm]	Angle [deg]
Old	M1	∞	-24.104	18.258	-6.000
	M2	∞	85.897	18.258	-174.000
	M3	50 mm	0.000	-0.000	6.000
	M4	50 mm	59.359	0.517	174.493
	PPKTP	—	24.406	-0.000	-178.854*
New	M1	∞	24.104	18.258	-174.000
	M2	∞	-85.897	18.258	-6.000
	M3	50 mm	0.000	-0.000	174.000
	M4	50 mm	-59.359	0.517	5.507
	PPKTP	—	-24.406	-0.000	-1.146*

crystal. It is hoped that the larger overall footprint should also make the installation of a remotely actuatable translation stage on the oven easier. Similar cavities are currently under test at MIT and The ANU.

The refractive index of the PPKTP crystal is different for the two wavelengths used. The cavity optics were positioned based on calculations using the average of the two indices. Hence, neither field will be incident exactly in the centre of the optics. However, assuming ideal mirrors and perfect alignment, the largest offset is of order 0.1 mm (0.5 mm with the crystal removed).

The differing refractive indices also dictate that the two cavity eigenmodes do not overlap. Again, this effect should be negligible and has been present in all OPOs to date.

4 Mirrors

We now present the desired mirror specifications.[2] We currently intend to purchase off-the-shelf substrates from Laseroptik. Previously, polishing was carried out by Photon LaserOptik with coatings provided by Laseroptik. Results were acceptable.

Mirror M2 is designed to be thinner than the other optics to increase the resonant frequency of the PZT actuator attached to it.

[2]Excepting the 532 nm reflectivity of M1, these values are identical to those in E1000023-V4.

4.1 Material

Corning HPFS 7980 (high purity fused silica, UV grade)
Grade 0A (Low inclusion class: <0.3 mm^2 cross section, 0.1 mm max. size; Homogeneity <1 ppm)

4.2 Dimensions

M1
FLAT-FLAT
Diameter: 12.7 mm +0/-0.1 mm
Thickness (thick edge): 6.35 mm ± 0.1 mm
Wedge: 30 ± 5 arcminute

M2
FLAT-FLAT
Diameter: 12.7 mm +0/-0.1 mm
Thickness (thick edge): 3.175 mm ± 0.1 mm
Wedge: 30 ± 5 arcminute

M3
PLANO-CONCAVE
Diameter: 12.7 mm +0/-0.1 mm
Thickness (edge): 6.35 mm ± 0.1 mm
Inner ROC (Side1): R1 = -50 mm ± 0.5 mm (1%)
Outer ROC (Side2): FLAT

M4
PLANO-CONCAVE
Diameter: 12.7 mm +0/-0.1 mm
Thickness (edge): 6.35 mm ± 0.1 mm
Inner ROC (Side1): R1 = -50 mm ± 0.5 mm (1%)
Outer ROC (Side2): FLAT

4.3 Surface roughness

Side 1
Super-polished
<1 Angstrom over central 80% of diameter with 10-5 scratch-dig; best effort for 0/0 20-10 scratch-dig outside central 80% of diameter.

Side 2
<5 Angstrom over central 80% of diameter.

4.4 Surface figure

Side 1
Flat < $\lambda/10$ at 632.8 nm over central 80%

Side 2
Flat $< \lambda/4$ at 632.8 nm over central 80%

4.5 Coating

Wavelength: 1064 nm and 532 nm
Polarisation: s (for both 1064 nm and 532 nm)
AOI: 6 degrees

M1
-Side 1
R@1064nm = 87.5% ± 1%
R@532nm= 87.5% ± 1%
-Side 2
AR@1064 <0.1%
AR@532 <0.2%

M2
-Side 1
R@1064 = 99.85% ± 0.05%
HR@532 >99.9%
-Side 2
AR@1064 <0.1%
AR@532 <0.2%

M3
-Side 1 (concave)
HR@1064 >99.99% (best effort)
HR@532 >99.9%
-Side 2 (flat)
AR@1064 <0.1%
AR@532 <0.2%

M4
-Side 1 (concave)
HR@1064 >99.99% (best effort)
HR@532 >99.9%
-Side 2 (flat)
AR@1064 <0.1%
AR@532 <0.2%

The reflectivities specified for M1 are derived assuming losses identical to those measured in [2] (i.e. equivalent mirrors with power transmissivities of 0.046 at 532 nm and 0.0026 at 1064 nm). Parameters suitable for modelling purposes are given in Table 3.

Table 3: Mirror reflectivities used in numerical models. All losses are assigned to M2.

Parameter	532 nm	1064 nm
R_1	0.875	0.875
R_2	0.954	0.9974
R_3	1	1
R_4	1	1

5 Nonlinear Crystal

The dimensions of the PPKTP crystal are shown in Figure 4. Useful parameters are listed in Table 4. The effects of the wedge have been included in all aspects of the cavity design. All calculations are performed assuming operation at 35°C. This detail has little bearing on the conclusions drawn. Crystals will be purchased from Raicol Crystals.

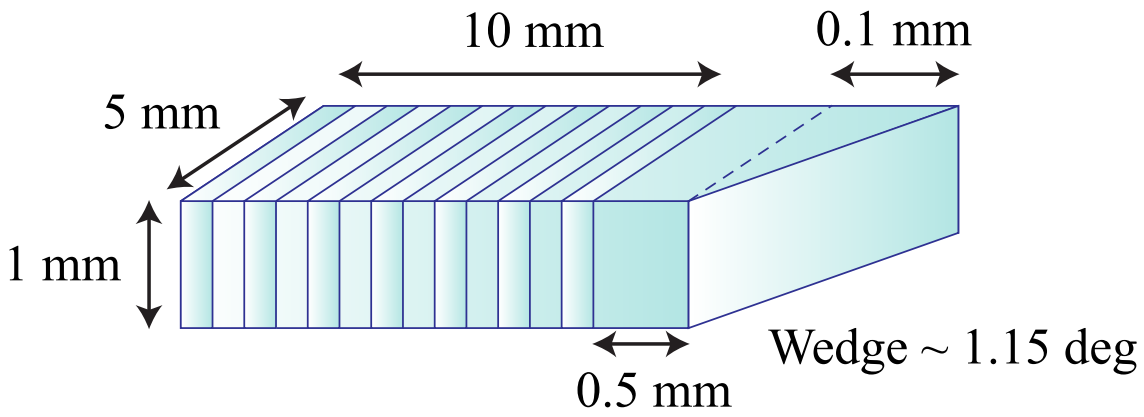

Figure 4: Dimensions of the OPO's nonlinear crystal. Note that the wedge angle was not changed to 1.43°. This appears to be an error on the part of Photon Laseroptik. (See email correspondence with Terry McRae.) Diagram adapted from [2].

Table 4: Parameters of the nonlinear crystal. The AR coating is designed for 0 deg aoi. The nominal length of the crystal assumes that the beam is propagating along its centreline.

Parameter	532 nm	1064 nm	Source
AR power reflectivity	$< 0.5\%$	$< 0.1\%$	[3]
Nominal length	10.505 mm		See Fig. 4
Refractive index, n	1.8894	1.8302	[4]
$\partial n/\partial T$	2.4188×10^{-5}	1.4774×10^{-5}	[5]
Thermal expansion coefficient α	6.7×10^{-6}		[5]
Thermal expansion coefficient β	11×10^{-9}		[5]

Assuming an operating temperature of 35 °C, the length of the crystal is 10.550718455 mm and the refractive indices are 1.88964188 at 532 nm and 1.83034774 at 1064 nm.[3]

[3]Superfluous digits given for those who wish to obtain exact agreement with my model.

6 Mechanical design

6.1 Metal v. glass

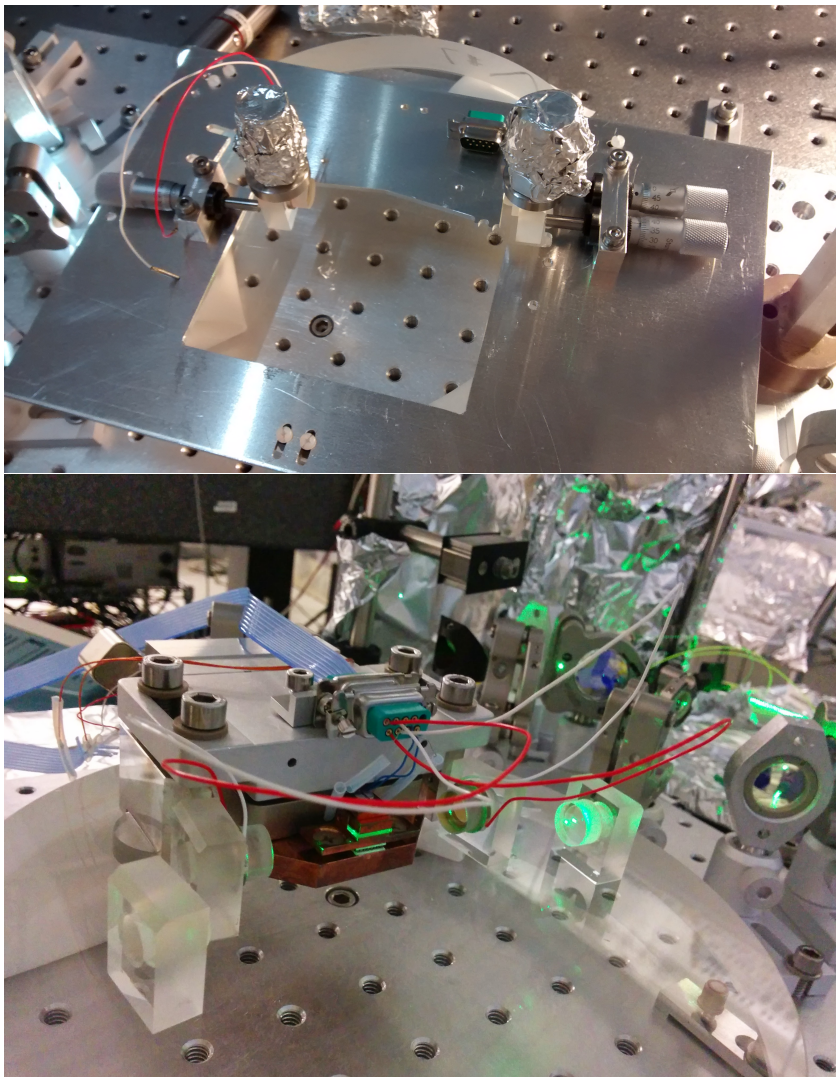

Figure 5: The MIT prototype glass OPO under construction (upper) and in use (lower).

6.1.1 Ease of construction

Building on experience gained at The ANU, an all-glass, quasi-monolithic OPO cavity was constructed at MIT (see Figure 5). This project was successful and informed us of the preparation, tooling and time required to build an OPO cavity in this way. Ultimately, given our requirements (see below), we feel that the additional investment demanded by a monolithic construction is not justified.

6.1.2 Length noise

Any length noise of the OPO cavity is converted into quadrature fluctuations of the squeezed ellipse and, consequently, reduced squeezing performance.

The coherent locking scheme relies on the coherent locking field (CLF) being a valid proxy for the squeezed field. In particular it should have a fixed phase relationship so that it may be used to control the squeeze angle relative to interferometer light. However, due to its detuning, the phase of CLF does not change in the same way as that of the squeezed field when the OPO cavity length varies, i.e. it is not a good sensor.[4] This leads to phase noise which cannot be suppressed even with ideal control loops (see Table 5).

Table 5: Phase change sensed by the squeezed light and CLF as OPO cavity length varies. Due to the detuning of the CLF field its phase response is different to that of the squeezed light, leading to phase noise which cannot be suppressed even with infinite loop gain/bandwidth. Values are given for the H1 squeezer, a VOPO cavity with the same green finesse as the H1 OPO and a VOPO with green finesse which has been increased by a factor of 2 (our baseline design). The CLF frequencies 1.3 MHz and 3.1 MHz were considered for the VOPO, with 3.1 MHz eventually preferred. 14.12 MHz is the frequency used in the VOPO prototype at MIT. 29.5 MHz was used in the H1 experiment.

	f	H1		VOPO low $\mathcal{F}$		VOPO high $\mathcal{F}$	
	[MHz]	[mrad/nm]		[mrad/nm]		[mrad/nm]	
		Sensed	Unsensed	Sensed	Unsensed	Sensed	Unsensed
Squeezing	0	99.7	—	99.7	—	129.0	—
CLF	1.3	98.6	1.1	98.1	1.6	127.3	1.7
	3.1	91.5	8.2	93.3	6.4	122.0	7.0
	14.12	67.7	32.0	61.2	38.5	86.9	42.1
	29.5	49.5	50.2	46.0	53.7	72.2	56.8

The magnitude of the reduction in sensitivity to cavity length noise with reduced CLF detuning was not appreciated during the initial stages of our design when a quasi-monolithic glass cavity was investigated. With our chosen CLF frequency (3.1 MHz) the influence of cavity length noise is more than five times smaller than previously assumed.

To achieve 6 dB of squeezing, the total phase noise from all sources should be less than 30 mrad RMS [6]. 10 dB requires less than 10 mrad [7]. We thus aim to to realise a phase noise contribution due to OPO cavity length fluctuations of $\lesssim$1 mrad.

Our chosen cavity design has an unsupressable length noise coupling of 7 mrad/nm. Hence, we require an RMS length noise below 0.14 nm.

The length noise of the H1 OPO (constructed from standard optomechanical mounts and housed, unsuspended, on an in-air optical table) may be inferred from [7] to be 0.6 nm. The residual length noise of the OMC has been measured to be around 1×10^{-4} nm RMS down to 100 mHz [8].

We thus believe that the length noise of a fixed-mount metal cavity, suspended on an isolated

[4] This issue also arises in the OMC and SRC.

platform, atop an ISI, in vacuum, should meet our requirement and not introduce a limiting source of squeezed quadrature fluctuations.

6.1.3 Reference cavity

It has been proposed that a suspended, in-vacuum OPO cavity may serve as a stable reference cavity to which the 532 nm pump field may be locked with high bandwidth, suppressing noise introduced, for example, on the squeezer table [9]. The alternative approach would be to lock the VOPO cavity to the incoming pump field using the cavity PZT, as was done in the H1 experiment.

The current control scheme entails feeding back to the OPO cavity length in order to lock the squeezing angle with respect to the interferometer signal quadrature. Therefore the stability of the cavity is related to the level of phase noise to be suppressed. We expect the level to be small and concentrated at low frequencies.

The stability of the field incident on the cavity will depend on the noise introduced by the optical fibres which deliver PSL light to the squeezer table and pump light to the VOPO. Components on the squeezer table will also induce phase noise (e.g. SHG cavity length fluctuations).

The control scheme we envision is flexible so that locking the laser to the cavity, the cavity to the laser or a frequency dependent combination of the two are all possible. The final choice will be made based on the in-situ noise environment. At this time, based on past experience, we present our best estimate of the final control topology.

6.1.4 Long-term stability

One of the benefits of glass is its low coefficient of thermal expansion. Here we examine the actuation range required to keep an all-metal cavity locked indefinitely given the measured diurnal temperature variation in the LIGO vacuum systems.

We plan to construct the cavity baseplate using Aluminium and install Noliac NAC2124-A01 PZTs on two of the mirrors (M2 and M4). Given the cavity length of the OPO (0.34 cm) and an assumed coefficient of thermal expansion of Aluminium (23×10^{-6}/K), the actuation range required to maintain the cavity on resonance in the presence of a given diurnal temperature variation is shown in Fig. 6.

Based on a random sampling of TCS HWS chamber temperature sensors (see Figure 7) and estimates based on the vertical displacement of the quad, one PZT is likely sufficient with two certainly providing adequate range.

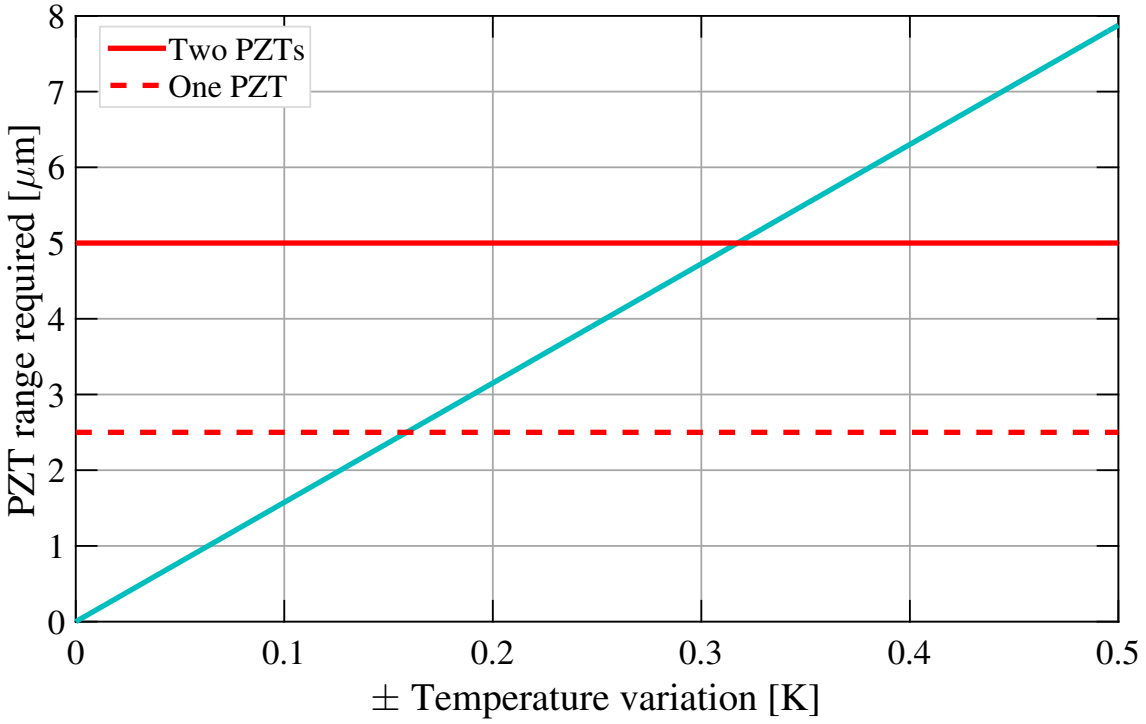

Figure 6: PZT range required to counteract diurnal temperature variations. For example, two PZTs can withstand variations of around ±300 mK. Assumed PZT range is 2.5 µm.

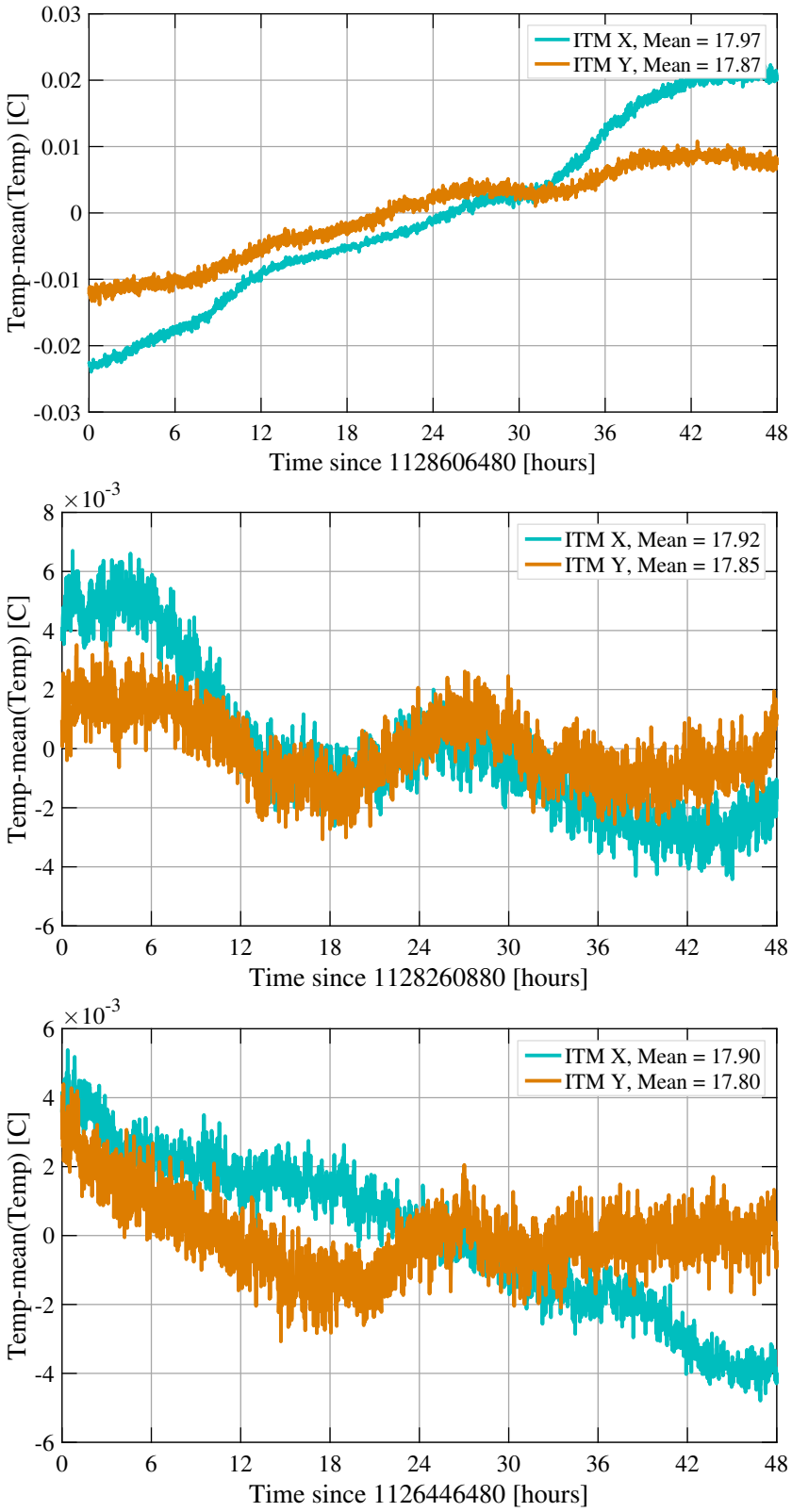

Figure 7: Temperature variation in the vertex area as measured by L1:TCS-ITMX_HWS_CHAMBERTEMPERATURESENSORA and L1:TCS-ITMY_HWS_CHAMBERTEMPERATURESENSORA at three times approximately three days (upper), one week (middle) and one month (lower) before the 14$^{\text{th}}$ of October 2015.

A Construction tolerances

A.1 Length

The cavity lengths are chosen to avoid the coincidence of higher order modes with the fundamental. Examining how far one can deviate from these nominal lengths before unwanted coincidence occurs defines the accuracy with which the cavity must be constructed.[5] We find that the separation of the curved mirrors is most critical. An error on this length of just 0.5 mm leads to an undesirable transverse mode spectrum. We thus place a tolerance of 0.1 mm on this length. In contrast, the other lengths are not at all critical, components could be placed with ±5 mm accuracy without negative consequences.

We must also consider the 1% uncertainty in mirror radii of curvature (see §4). To compensate for this unknown variation, the separation of the curved mirrors must be tunable by up to 0.5 mm.

A.2 Angle

Let us assert that the optical axis shall not move by more than 0.5 mm due to any misalignment. The mirror radii are 6.35 mm; the largest spot size is 0.3 mm.[6]

With this criterion we estimate a reasonable manufacturing tolerance by repeatedly applying random misalignments, drawn from a uniform distribution of specified width, to all four cavity mirrors and determining the beam spot offsets on all of the optics. If all offsets are less than 0.5 mm we deem the cavity acceptable. Fig. 8 shows results of applying this procedure in the sagittal plane. A pitch alignment (i.e. manufacturing) tolerance of around 1 mrad is required.

In the tangential plane we take the additional step of trying to restore good alignment through rotations of one of the cavity mirrors (M3) (see Fig. 9). The ability to correct errors in this way relaxes the required manufacturing tolerance to around 4 mrad. However, the corrective alignments (of around 7 mrad) must be achieved at the ±0.5 mrad level (see Fig. 10). For context, consider that a standard mirror mount has an actuation coefficient of ∼10 mrad per turn.

Based on these calculations, we aim to fix the locations of three of cavity mirrors, two flat, one curved, during manufacture and allow some adjustment of the other curved mirror. The range of this adjustment should not be less than 1 mm in translation and 10 mrad in angle.

[5] However, in the case of the separation between the two flat mirrors or flat mirror and curved mirror, the spot size in the crystal becomes too large before we hit a higher order mode coincidence.

[6] The crystal is 1 mm thick and 5 mm wide but is movable.

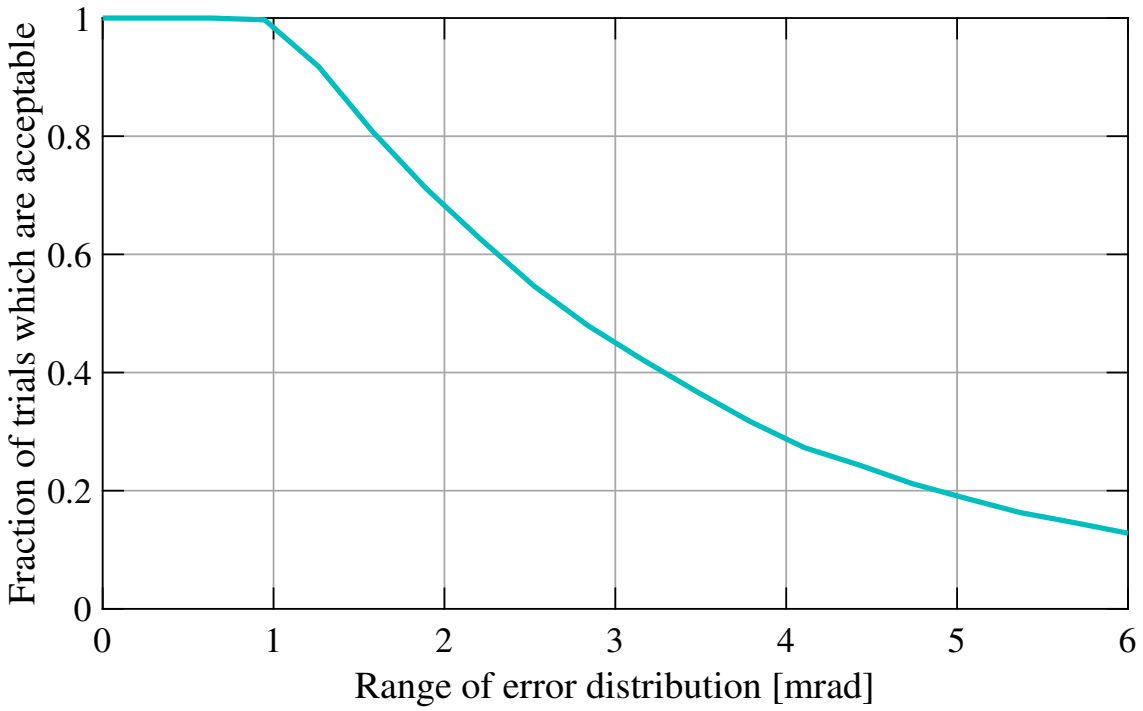

Figure 8: Fraction of 1000 trials which yield acceptable cavities when all mirrors are given different random misalignments in the sagittal plane drawn from a uniform distribution of width ranging from zero to ±6 mrad.

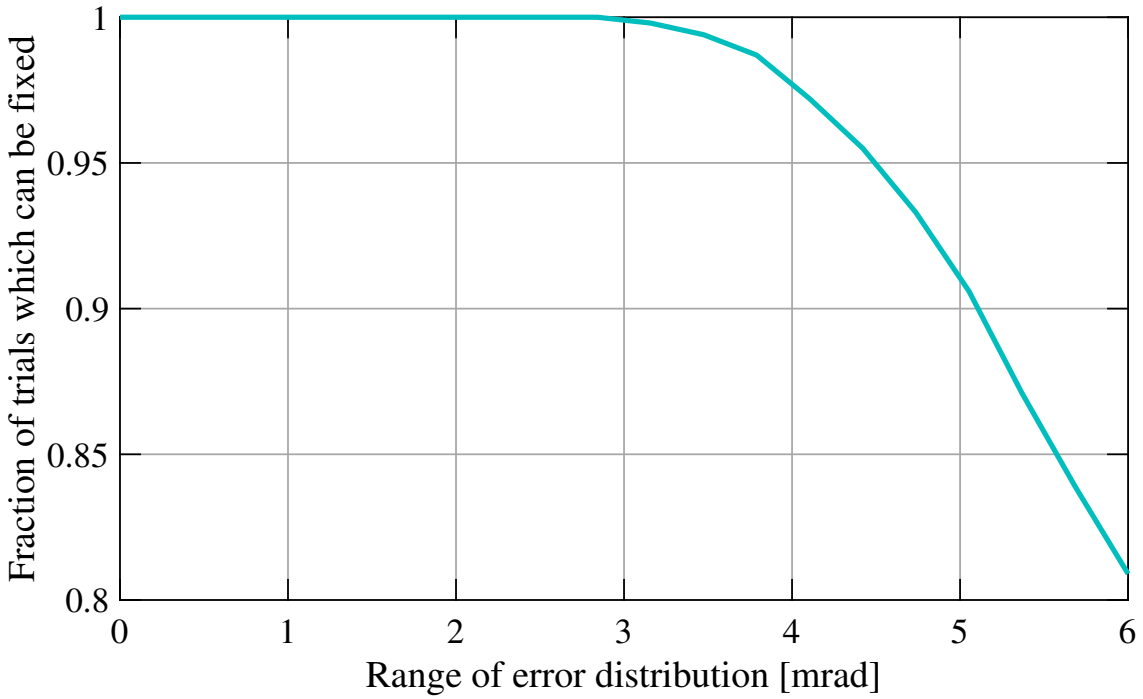

Figure 9: Fraction of 1000 trials which yield acceptable cavities when all mirrors are given different random misalignments in the tangential plane drawn from a uniform distribution of width ranging from zero to ±6 mrad and the alignment of one of the curved mirrors is subsequently aligned to compensate.

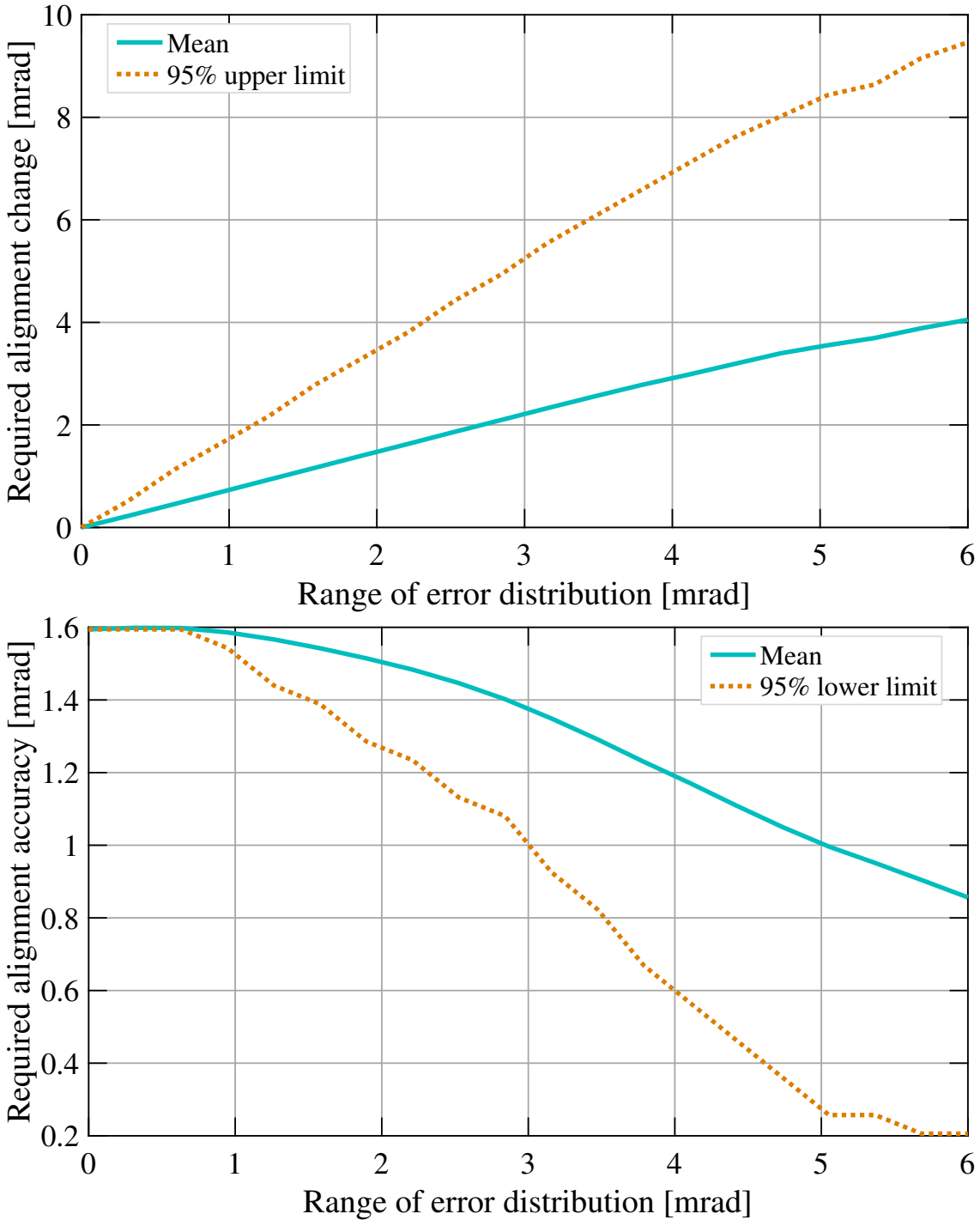

Figure 10: The alignment angles (upper axes) and accuracies (lower axes) required to compensate for random mirror misalignments. For example, if the error distribution has width ±5 mrad, the compensating mirror must be rotated by ∼3.5±1 mrad, if considering mean values.

B Mode matching

This section details telescopes which could be used to match light from the optical fibres to the VOPO cavity. We currently plan to employ connectorised aspheric collimators from Lightpath for this task. Results should be interpreted as proofs of concept rather than final designs.

B.1 1064 nm

In matching the CLF/seed beam to the OPO we will use Lightpath model 355230-FCAPC-1064. We note that the measured waist of this fibre was somewhat smaller than specified.

Telescope parameters may be found in Table 6. Beam spot size and Gouy phase as a function of propagation distance are shown in Fig. 11.

Table 6: Details of a telescope which could match the CLF/seed beam to the VOPO cavity.

Parameter	Value
q value on AR surface of M2	$0.05077 + 0.13509i$.
Fibre waist size	372 µm
Fibre waist position	0 m
Lens position	3 cm
Lens focal length	333.6 mm
M2 AR surface position	28.40 cm

B.2 532 nm

The pump fibre will be matched to the cavity using a custom (as yet untested) coupler based on Lightpath model 355230 - (FCPC/FCAPC/SMA) - 543. This coupler is designed to operate at 543 nm. For this exercise we use the nominal parameters at 543 nm.

Telescope properties are described in Table 7. Beam spot size and Gouy phase as a function of propagation distance are illustrated in Fig. 12. The relatively large separation between the coupler and first lens is present due to constraints imposed by the layout of the suspended VOPO injection platform.

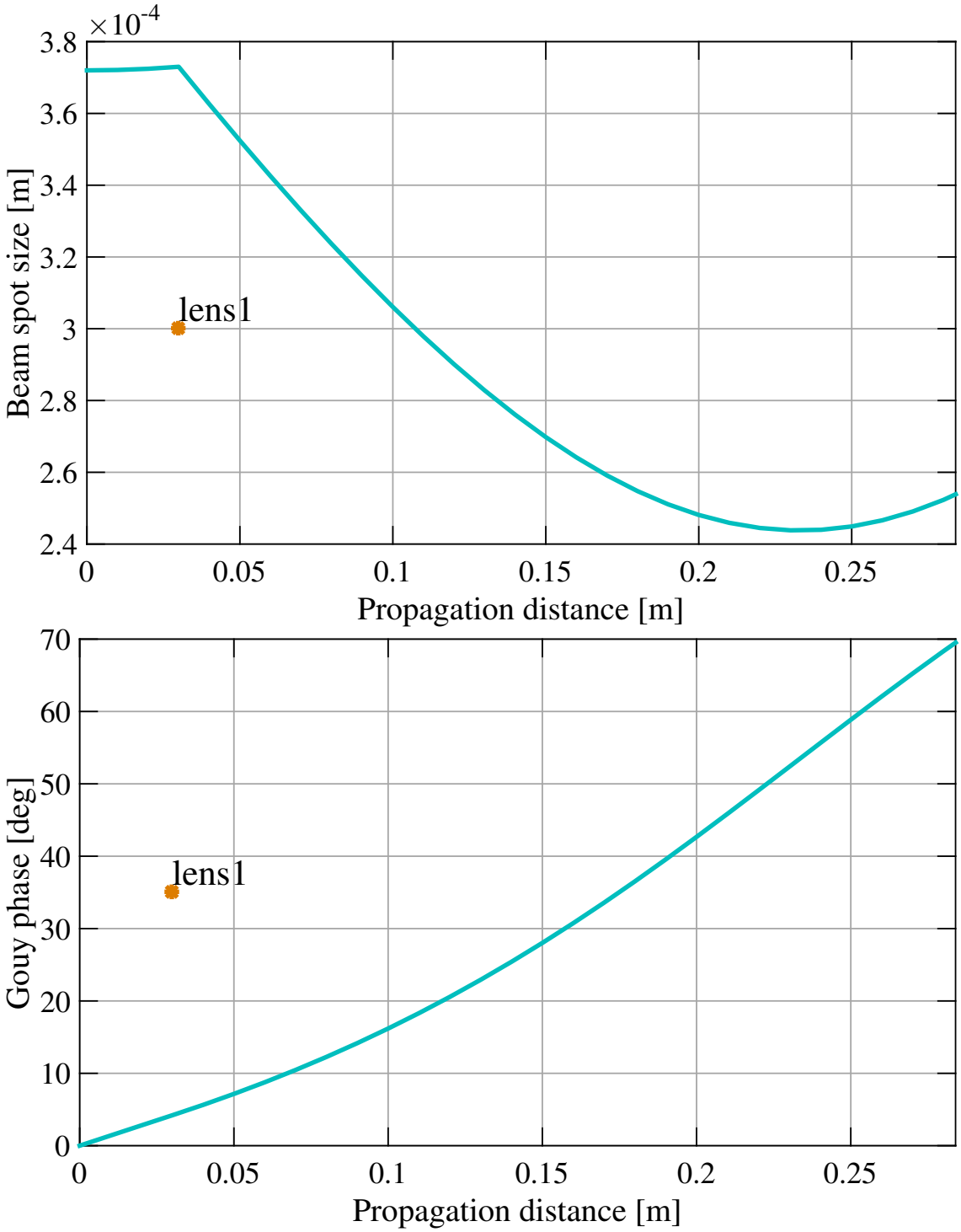

Figure 11: Beam spot size and Gouy phase of a telescope which could match light from the CLF/seed fibre to the VOPO cavity.

Table 7: Details of a telescope which could match the pump beam to the VOPO cavity.

Parameter	Value
q value on AR surface of M1	$-0.05923 + 0.13991i$.
Fibre waist size	450 µm
Fibre waist position	0 m
Lens 1 position	14.90 cm
Lens 1 focal length	217.1 mm
Lens 2 position	25.49 cm
Lens 2 focal length	-217.1 mm
M1 AR surface position	36.36 cm

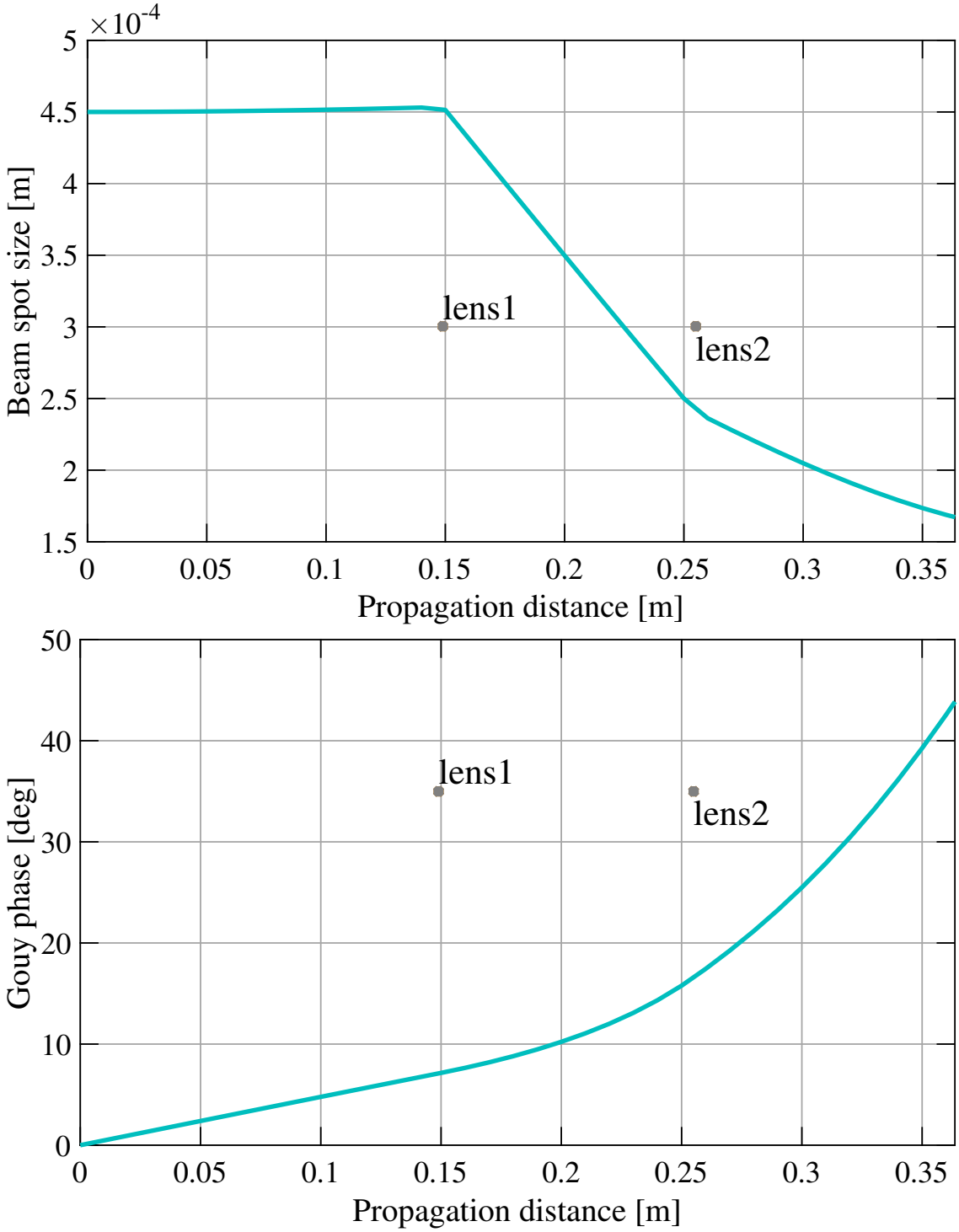

Figure 12: Beam spot size and Gouy phase of a telescope which could match light from the pump fibre to the VOPO cavity.

C Beam spot sizes and transverse mode spectra with PPKTP crystal removed

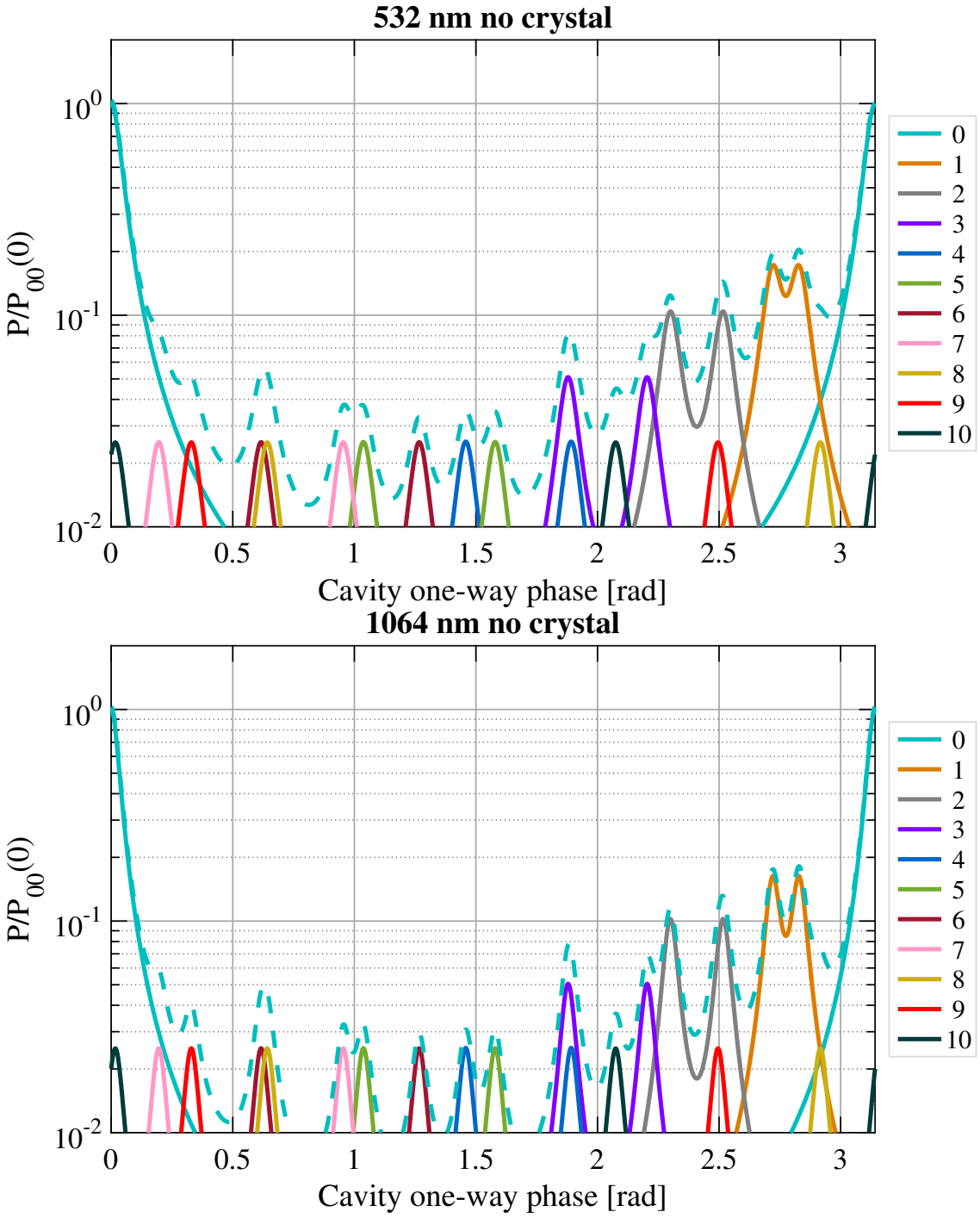

Figure 13: Simulated transverse mode spectrum of the VOPO cavity with the PPKTP crystal removed. Legend values indicate mode order. For each order, peaks are only drawn for the highest and lowest frequency modes (e.g. 20 and 02 but not 11). The relative powers in each mode were chosen arbitrarily. The total power is given by the dashed trace.

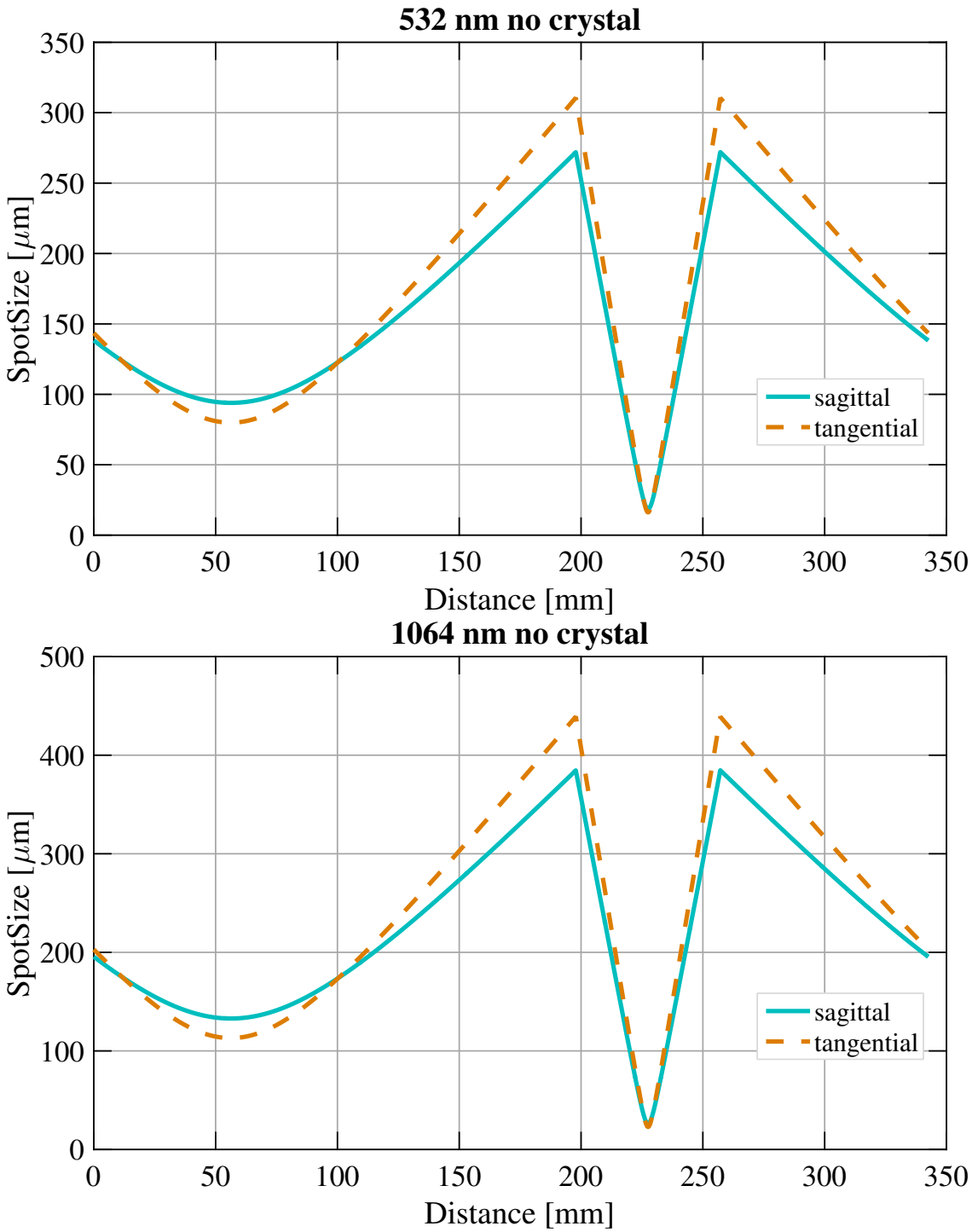

Figure 14: Beam spot size as a function of distance from M1 for the VOPO cavity when the PPKTP crystal has been removed.

D Escape efficiency

The escape efficiency of an OPO is one of the critical parameters defining the level of squeezing it can produce. Escape efficiency, η is defined as

$$\eta = \frac{\gamma^{\text{out}}}{\gamma}, \tag{1}$$

where γ^{out} and γ are the cavity decay rates associated with the output coupler and the entire cavity, respectively, at the squeezing wavelength.

The decay rate of an effective reflectivity r is calculated by considering the field amplitude in the cavity as a function of the number of round trips n_{rt}

$$E(n_{\text{rt}}) = E_0 \times r^{n_{\text{rt}}}. \tag{2}$$

Converting this expression to a function of time and rearranging into canonical form we have

$$\begin{aligned} E(t) &= E_0 \times r^{t/t_{\text{rt}}} &(3)\\ &= E_0 \times \exp\left(-\gamma t\right), &(4)\end{aligned}$$

where t_{rt} is the cavity round-trip time. Comparing terms in the previous expression the decay rate is found to be

$$\gamma = \frac{-\ln(r)}{t_{\text{rt}}} = \frac{-\ln(R)}{2t_{\text{rt}}}. \tag{5}$$

Equation (5) may be simplified by expanding the logarithm to first order and assuming that $1 - R = T \ll 1$

$$\gamma \simeq \frac{1-r}{t_{\text{rt}}} = \frac{1-\sqrt{R}}{t_{\text{rt}}} \simeq \frac{T}{2t_{\text{rt}}}. \tag{6}$$

However, care must be taken in checking the validity of these approximations, relative errors of around 10% are typical for our parameters.

Modelling the OPO cavity as a two mirror device where all losses are associated with the second mirror, escape efficiency may be written in the more experimentally-friendly form

$$\eta = \frac{\ln(R_1)}{\ln(R_1 R_2)}. \tag{7}$$

In practice, R_1 is determined via independent measurement and R_2 is found through experimental measurements of the reflected power on and off resonance [2].[7]

$$\frac{P_{\text{refl}}^{\text{on res}}}{P_{\text{refl}}^{\text{off res}}} = \left(\frac{(r_1 - r_2)(1 + r_1 r_2)}{(r_1 + r_2)(1 - r_1 r_2)}\right)^2. \tag{8}$$

Recent measurements of these quantities on a prototype VOPO cavity are given in Table 8.

[7] We note that care must be taken to account for the presence of higher order modes.

Table 8: Experimental measurement of escape efficiency on a prototype VOPO. This cavity had a CLF mirror with an unusually high reflectivity of 0.9996. Derived parameters are marked with an asterisk.

Parameter	Value
R_1	0.845
$P_{\text{refl}}^{\text{on res}}/P_{\text{refl}}^{\text{off res}}$	0.9657
R_2^*	0.99853
Escape efficiency*	99.1%

E Thermal lens

The thermal lens induced in the PPKTP crystal may be modelled as a thin lens located at the centre of the crystal. Subdividing the crystal into discrete lengths along the direction of propagation and summing the powers of the lenses formed in each section, an approximate (assuming only radial heat flow) formula for the power $(1/f)$ of the total thermal lens in the PPKTP crystal is [10, 11]

$$p = \frac{\alpha(\partial n/\partial T)P_{\text{cavity}}}{\pi K_c}\int_{-\text{lengthCrystal}/2}^{\text{lengthCrystal}/2}\frac{1}{\omega^2(z)}\mathrm{d}z \tag{9}$$

$$= \frac{\alpha(\partial n/\partial T)P_{\text{cavity}}}{\pi K_c}\frac{2z_R}{\omega_0^2}\arctan\left(\frac{L_{\text{crystal}}}{2z_R}\right), \tag{10}$$

where α is the absorption coefficient, P_{cavity} is the incident (circulating cavity) power, z_R is the Rayleigh range and K_c is the thermal conductivity. Evaluating this expression for the 532 nm pump light with the parameters given in Table 9 gives results of order 80 mm. Although seemingly short, this focal length has little effect on the properties of the cavity mode as the lens is located at a ∼20 µm beam waist. We therefore ignore thermal lenses in our evaluation of cavity geometries.

Table 9: Parameters (not given elsewhere in this document) used in evaluating the importance of thermal lenses in the PPKTP crystal. Selected values are on the conservative side of realistic so that we should overestimate the lensing effect.

Parameter	Value
α	0.2 m^{-1}
P_{input}	100 mW
K_c	3 $\text{Wm}^{-1}\text{K}^{-1}$
ω_0	15 µm

F Optimal spot size

The optimal spot size for an OPO is discussed by Fejer in [12], the pertinent information is drawn from the classic Boyd and Kleinmann paper [13].

In short, the optimal spot size for the pump beam is given by

$$\xi = \frac{l}{2z_R} = \frac{l\lambda_{\rm pump}}{2n_{\rm crystal}\pi\omega_0^2} = 2.84, \tag{11}$$

where l is the length of the crystal and z_R is the Rayleigh range. The maximum is relatively soft so that $\xi = 1$, an oft espoused rule of thumb, results in only a 20% drop in parametric gain. Rearranging the above we find

$$\omega_0(\xi) = \left(\frac{l\lambda_{\rm pump}}{2n_{\rm crystal}\pi\xi}\right)^{1/2}. \tag{12}$$

For our crystal parameters

$$\omega_o(2.84) = 12.9\ \mu\text{m},$$
$$\omega_o(1) = 21.7\ \mu\text{m}.$$

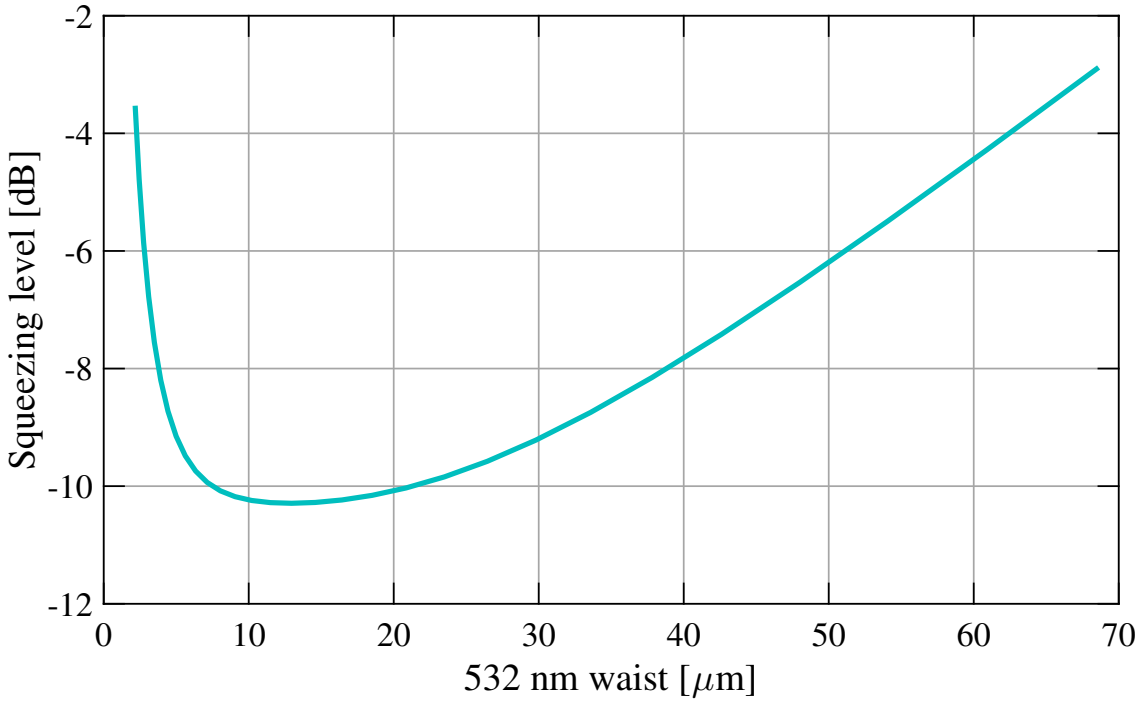

Figure 15: Squeezing level as a function of pump beam waist size (assumed to be centred in the crystal). Plot is made using a list of assumed parameters roughly, but not exactly, representative of our squeezers.

G Methods

All calculations were performed using ABCD matrices. To verify these results an OptoCad[14] model was also constructed. Appropriate details are provided in this section.

G.1 ABCD matrices

- Propagation over distance d.

$$M_{\text{prop}} = \begin{pmatrix} 1 & d \\ 0 & 1 \end{pmatrix} \tag{13}$$

- Refraction at curved (ROC=R) dielectric interface tilted by angle θ [15][8]. R need not be the same in both planes. $n_r = n_2/n_1$.

$$M_{\text{refrac,sagittal}} = \begin{pmatrix} 1 & 0 \\ \frac{\cos(\theta) - \sqrt{n_r^2 - \sin^2(\theta)}}{-R n_r} & \frac{1}{n_r} \end{pmatrix} \tag{14}$$

$$M_{\text{refrac,tangential}} = \begin{pmatrix} \frac{\sqrt{n_r^2 - \sin^2(\theta)}}{n_r \cos(\theta)} & 0 \\ \frac{\cos(\theta) - \sqrt{n_r^2 - \sin^2(\theta)}}{-R\cos(\theta)\sqrt{n_r^2 - \sin^2(\theta)}} & \frac{\cos(\theta)}{\sqrt{n_r^2 - \sin^2(\theta)}} \end{pmatrix} \tag{15}$$

- Mirror with radius of curvature R_{eff}. In the tangential (cavity) plane $R_{\text{eff}} = R\cos(\theta_{\text{aoi}})$; in the sagittal (normal-to-cavity plane) plane $R_{\text{eff}} = R/\cos(\theta_{\text{aoi}})$. For normal incidence $R_{\text{eff}} = R$.

$$M_{\text{mirror}} = \begin{pmatrix} 1 & 0 \\ -2/R_{\text{eff}} & 1 \end{pmatrix} \tag{16}$$

G.2 g factor and Gouy phase from ABCD matrix

A nice reference on this material is [16]. Note that I use the one-way phase, defined as half of the round-trip phase.

$$g = \frac{A + D + 2}{4} \tag{17}$$

$$\Phi_{\text{Gouy}} = \cos^{-1}\left(\text{sign}(B)\sqrt{g}\right) \tag{18}$$

G.3 R, ω and Eigen-q at the start of the ABCD system

$$R = \frac{2B}{D - A} \tag{19}$$

$$\omega = \left[\frac{(\lambda/\pi)^2 |B|^2}{1 - (A + D)^2/4}\right]^{1/4} \tag{20}$$

$$q = \left(\frac{1}{R} - i\frac{\lambda}{\pi\omega^2}\right)^{-1} \tag{21}$$

[8] N.B. I use a different sign convention for the radius of curvature.

G.4 Alignment sensitivity analysis

A misaligned optical element may be described by the 3×3 matrix [17, 18]

$$M = \begin{pmatrix} A & B & \Delta x \\ C & D & \Delta\theta \\ 0 & 0 & 1 \end{pmatrix}, \tag{22}$$

where A, B, C and D are the elements of the standard 2×2 ABCD matrix associated with the element and Δx and $\Delta\theta$ describe the offset and angular deviation of a beam propagating along the optical axis after interaction with the misaligned element. The calculation of these new matrix terms is outlined in [19] and [20].[9] Example matrices for spherical mirrors follow [22, 23]:

$$M_{\text{mirror}}(R, \delta x) = \begin{pmatrix} 1 & 0 & 0 \\ -2/R_{\text{eff}} & 1 & 2\delta x/R_{\text{eff}} \\ 0 & 0 & 1 \end{pmatrix}, \tag{23}$$

$$M^{\text{sagittal}}_{\text{mirror}}(R, \delta\theta) = \begin{pmatrix} 1 & 0 & 0 \\ -2/R_{\text{eff}} & 1 & 2\delta\theta\cos(\theta_{\text{aoi}}) \\ 0 & 0 & 1 \end{pmatrix}, \tag{24}$$

$$M^{\text{tangential}}_{\text{mirror}}(R, \delta\theta) = \begin{pmatrix} 1 & 0 & 0 \\ -2/R_{\text{eff}} & 1 & 2\delta\theta \\ 0 & 0 & 1 \end{pmatrix}. \tag{25}$$

In this formalism the vector describing beam position and angle is augmented with a 1 as its final entry so that calculations are of the form

$$\begin{pmatrix} x_{\text{out}} \\ \theta_{\text{out}} \\ 1 \end{pmatrix} = M \begin{pmatrix} x_{\text{in}} \\ \theta_{\text{in}} \\ 1 \end{pmatrix}. \tag{26}$$

In cavities with greater than two mirrors, care must be taken to preserve the correct coordinate system on reflection (see Figure 16) [24]. This may be accomplished by multiplying each mirror matrix by a second coordinate matrix, i.e. $M'_{\text{mirror}} = M_{\text{coordinate}} M_{\text{mirror}}$ where

$$M^{\text{sagittal}}_{\text{coordinate}} = \begin{pmatrix} 1 & 0 & 0 \\ 0 & 1 & 0 \\ 0 & 0 & 1 \end{pmatrix}, M^{\text{tangential}}_{\text{coordinate}} = \begin{pmatrix} -1 & 0 & 0 \\ 0 & -1 & 0 \\ 0 & 0 & 1 \end{pmatrix}. \tag{27}$$

Under this proviso calculations proceed exactly as with standard ABCD matrices.

We calculate the round-trip matrix, eigenvector and beam spot position on every optic as a each mirror is individually misaligned, yielding mirror tilt/offset to spot position transfer coefficients. We define the misalignment sensitivity to be the largest of these coefficients.

Note that we do not account for changes in the angles of incidence and refraction at the crystal due to mirror tilts/offsets. This simplification was checked using OptoCad and found to have negligible impact.

[9] Although the latter reference uses a slightly different formalism [21].

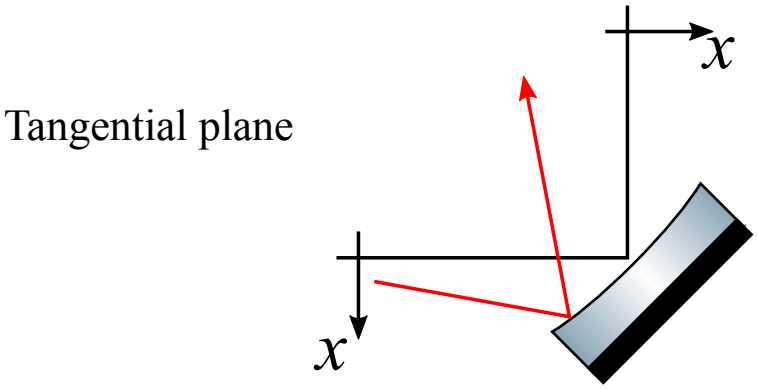

Figure 16: Positive angles and offsets in the tangential plane become negative upon reflection.

Beam spot position on the mirrors is preferred to e.g. the tilt and displacement of the waist relative to some nominal input beam as we are primarily interested in tolerances which must be attained during construction of the fixed cavity. In operation the input beam can be aligned to whatever cavity axis is formed (within reason). Figure 17 shows typical output of the simulation.

We note that the perturbation of the eigenmode is easily obtained from the elements of the round-trip matrix via

$$x = \frac{(1-D)\Delta x + B\Delta\theta}{2-A-D} \tag{28}$$

$$\theta = \frac{(1-A)\Delta\theta + C\Delta x}{2-A-D} \tag{29}$$

G.5 Analytical expressions

The majority of this work was undertaken using numerical means. However, it is instructive to examine some of the quantities considered analytically. These expressions neglect the wedge of the PPKTP crystal. The cavity is thus symmetric about its mid-plane.

G.5.1 g factor

The g factor of a bow-tie cavity, as described above, is

$$g = \frac{(L_1 - \mathrm{ROC})(L_2 - \mathrm{ROC})}{\mathrm{ROC}^2} \tag{30}$$

$$= \left(1 - \frac{L_1}{ROC}\right)\left(1 - \frac{L_2}{ROC}\right), \tag{31}$$

where L_1 is the short/direct distance between the curved mirrors, and L_2 is the distance between the curved mirrors travelling via the two flat mirrors. This expression is reminiscent of that of a standard two-mirror cavity.

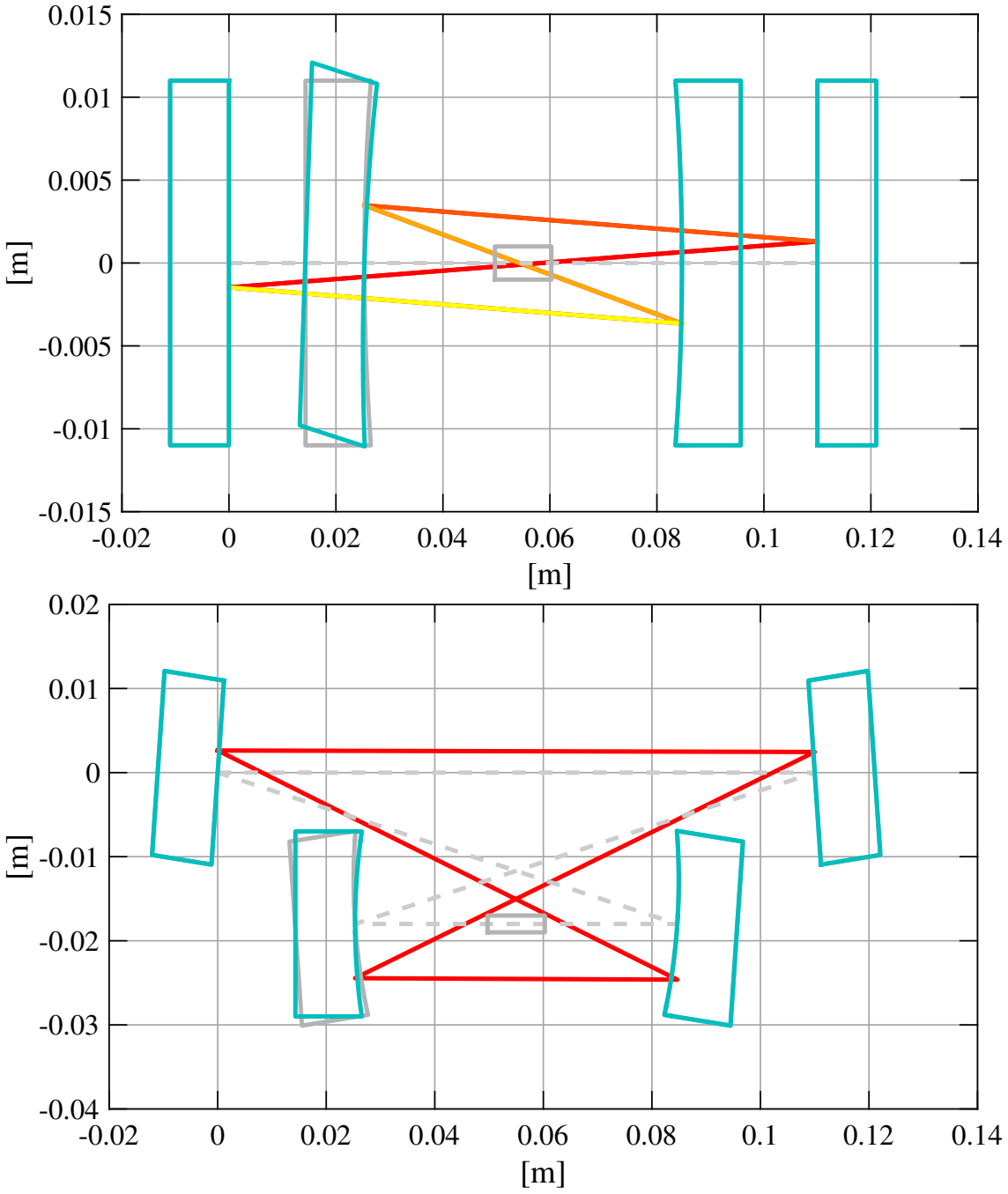

Figure 17: Eigenmode perturbation for tilts of M3 in the sagittal (upper axes) and tangential (lower axes) planes. These diagrams neglect the crystal wedge; values reported above do not. Diagrams are not to scale.

If one includes the non-linear crystal one simply replaces the distance between the curved mirrors with the effective length $L_1^{\text{eff}} = L_1 - L_{\text{crystal}} + L_{\text{crystal}}/n_{\text{crystal}}$.[10]

[10]To understand this concept of effective length simply plot beam spot size as a function of position on propagation through a waist in two cases: 1) where the waist is contained in the same refractive index as the surroundings and 2) where the waist is contained within a glass crystal. Note how the waist position is

The difference in g factors between a cavity containing a nonlinear crystal and one without is

$$\Delta g = g_{\text{crystal}} - g_{\text{no crystal}} \tag{32}$$

$$= L_{\text{crystal}} \left(\frac{1}{n_{\text{crystal}}} - 1 \right) \times \frac{1}{\text{ROC}} \left(1 - \frac{L_2}{\text{ROC}} \right). \tag{33}$$

Thus we see that to have a cavity which is stable both with and without a crystal it is advantageous to utilise a larger ROC.

In order to examine the accuracy with which one must control the various cavity lengths it is also useful to record the following derivatives

$$\frac{\partial g}{\partial L_1} = -\frac{1}{\text{ROC}} \left(1 - \frac{L_2}{\text{ROC}} \right), \tag{34}$$

$$\frac{\partial g}{\partial L_2} = -\frac{1}{\text{ROC}} \left(1 - \frac{L_1^{\text{eff}}}{\text{ROC}} \right). \tag{35}$$

It is not immediately obvious from these expressions but, consulting the tables presented above, the g factor is significantly more sensitive to variations in L_1^{eff} than L_2. This increased sensitivity also applies to higher order mode spacing.

G.6 Output of OptoCad model

These data are included more for personal reference than public consumption. Those wishing to decode the output should consult the OptoCad documentation [14].

Sections G.6.7 and G.6.8 tabulate the data used to position and size the holes in the OPO box. Figure 19 presents the corresponding model. Two input beams were used to capture all beams which may enter or exit the cavity – one beam entering in the standard propagation direction (black lables) and one in the reverse direction (red labels). We use 1064 nm beams as they have the largest spots and take the average refractive index for the crystal. Mirror substrates are assumed to have a refractive index of 1.5 for both wavelengths.

displaced.

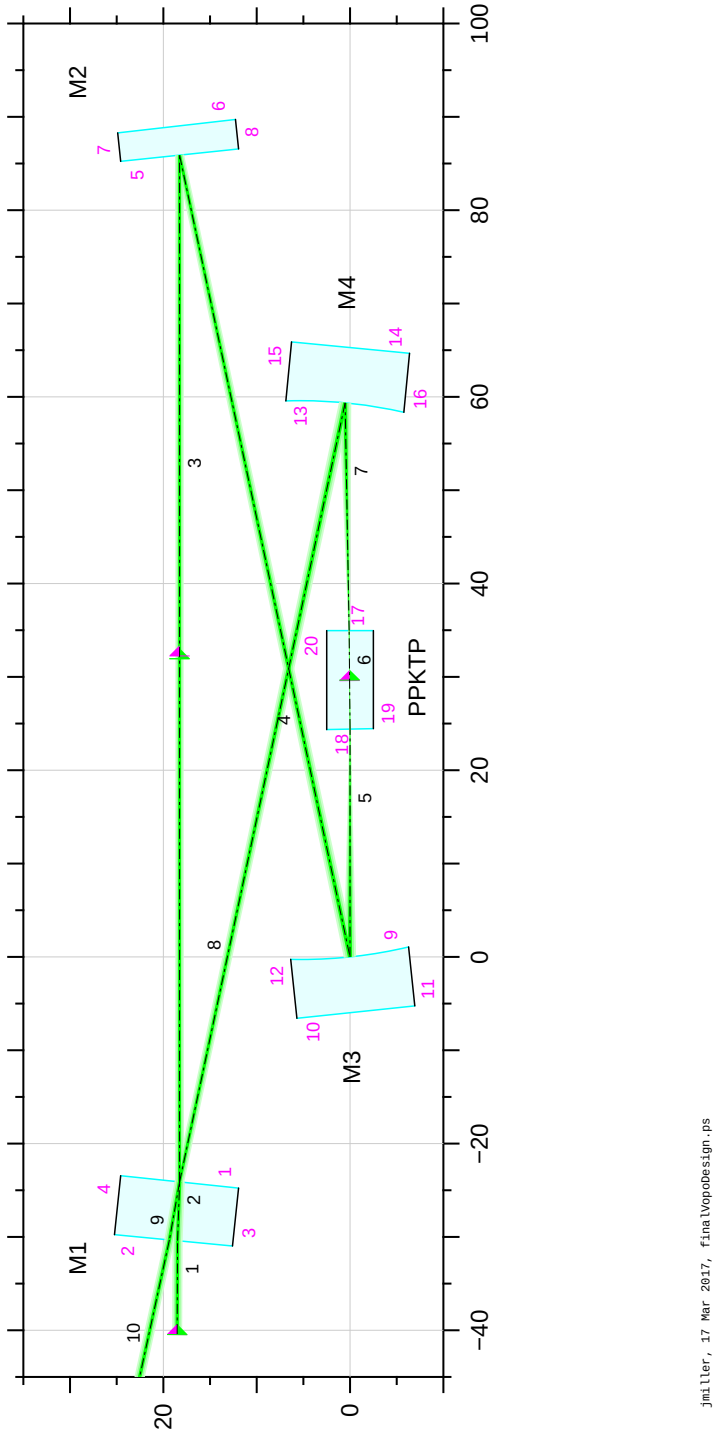

Figure 18: OptoCad model of the VOPO, in this instance for the 532 nm pump field. Black numbers correspond to the ray segment labels used in the following tables.

G.6.1 532 nm with crystal

#rs	label	ipp[mm]	rd[mm]	an2[deg]	w0t[mm]	w0s[mm]	w2t[mm]	w2s[mm]	z2t[mm]	z2s[mm]	x2[mm]	y2[mm]	Gp2t[deg]	Gp2s[deg]
1	+ M1	10.00009674E+0	-439.4599330E-3	5.247979444E+0	180.0000000E-3	180.0000000E-3	180.2456904E-3	180.2456904E-3	10.00009674E+0	10.00009674E+0	-30.40640984E+0	18.47856249E+0	1.495955217E+0	1.495955217E+0
2	# M1	9.459119252E+0	-16.8198788E-15	3.995931750E+0	180.4213420E-3	180.0000000E-3	180.9164800E-3	180.4953468E-3	21.37653115E+0	21.30622461E+0	-24.10418747E+0	18.25803601E+0	2.119975204E+0	2.122895745E+0
3	# M2	109.9999435E+0	7.149804869E-3	-6.000273783E+0	148.7821633E-3	159.1783317E-3	160.9324219E-3	169.0829098E-3	53.89676486E+0	53.59817279E+0	85.89655858E+0	18.26514664E+0	22.81760766E+0	20.18117397E+0
4	# M3	87.81634650E+0	-6.727917992E-3	6.007983409E+0	148.7821633E-3	159.1783317E-3	219.4361215E-3	219.0224179E-3	141.7131114E+0	141.4145193E+0	-702.8087596E-6	6.691109068E-3	35.26964161E+0	32.01899654E+0
5	+ PPKTP	24.40684437E+0	6.194414893E-6	-1.161455874E+0	21.09773233E-3	21.11640721E-3	30.85740764E-3	30.69251031E-3	-2.805472157E+0	-2.777505545E+0	24.40614065E+0	6.193176383E-6	54.07841549E+0	50.98864529E+0
6	# PPKTP	19.93793640E+0	-97.81745042E-3	531.1497646E-3	21.10085375E-3	21.11640721E-3	30.69303776E-3	30.85981291E-3	5.248265481E+0	5.302681154E+0	34.95685923E+0	97.81745042E-3	100.7955383E+0	97.66363209E+0
7	# M4	24.40705242E+0	8.095996080E-3	6.501723009E+0	21.09852262E-3	21.11640721E-3	219.2004367E-3	219.2529852E-3	27.18382509E+0	27.21323554E+0	59.36016663E+0	525.3635807E-3	119.7493252E+0	116.4893154E+0
8	# M1	85.32809022E+0	-7.678325670E-3	-5.999726217E+0	148.7821633E-3	159.1783317E-3	161.9063245E-3	170.1119080E-3	-56.10317859E+0	-56.40177066E+0	-24.10338487E+0	18.26567227E+0	131.7621160E+0	127.8861099E+0
8	# M1	85.32809022E+0	-7.678325670E-3	-5.999726217E+0	148.7821633E-3	159.1783317E-3	161.9063245E-3	170.1119080E-3	-56.10317859E+0	-56.40177066E+0	-24.10338487E+0	18.26567227E+0	131.7621160E+0	127.8861099E+0
9	+ M1	9.470659212E+0	439.9960664E-3	-4.495931750E+0	180.4213420E-3	180.0000000E-3	181.2513932E-3	180.8316463E-3	27.69030396E+0	27.61999742E+0	-30.32211772E+0	19.35396965E+0	2.742743953E+0	2.748566949E+0

G.6.2 1064 nm with crystal

#rs	label	ipp[mm]	rd[mm]	an2[deg]	w0t[mm]	w0s[mm]	w2t[mm]	w2s[mm]	z2t[mm]	z2s[mm]	x2[mm]	y2[mm]	Gp2t[deg]	Gp2s[deg]
1	+ M1	10.00009674E+0	-439.4599330E-3	5.247979444E+0	180.0000000E-3	180.0000000E-3	180.9807602E-3	180.9807602E-3	10.00009674E+0	10.00009674E+0	-30.40640984E+0	18.47856249E+0	2.983796325E+0	2.983796325E+0
2	# M1	9.459119252E+0	-16.8198788E-15	3.995931750E+0	180.4213420E-3	180.0000000E-3	182.3938293E-3	181.9732970E-3	21.37653115E+0	21.30622461E+0	-24.10418747E+0	18.25803601E+0	4.216982801E+0	4.222729516E+0
3	# M2	110.0030435E+0	-7.133795403E-3	-5.999709191E+0	206.9107079E-3	221.2196752E-3	224.9306935E-3	235.9529671E-3	53.89277782E+0	53.60706237E+0	85.89805162E+0	18.25094129E+0	23.51305445E+0	20.83747602E+0
4	# M3	87.81625555E+0	6.685575245E-3	5.992048086E+0	206.9107079E-3	221.2196752E-3	310.8308282E-3	309.5433958E-3	141.7090334E+0	141.4233179E+0	699.2774271E-6	-6.648904244E-3	36.10093448E+0	32.85235851E+0
5	+ PPKTP	24.40544237E+0	1.544523435E-6	-1.130149819E+0	29.88575569E-3	29.98156477E-3	44.38445077E-3	44.14064206E-3	-2.895637953E+0	-2.867835173E+0	24.40614074E+0	1.544214624E-6	54.50486172E+0	51.46491884E+0
6	# PPKTP	19.31230481E+0	-97.29536179E-3	528.3400483E-3	29.88983491E-3	29.98156477E-3	44.15406257E-3	44.38079125E-3	5.249695754E+0	5.302031448E+0	34.95685923E+0	97.29536179E-3	102.0395821E+0	98.82469796E+0
7	# M4	24.40522568E+0	-8.138256810E-3	6.483684518E+0	29.88684800E-3	29.98156477E-3	310.5006167E-3	309.8658826E-3	27.27279367E+0	27.30196018E+0	59.35860858E+0	509.2042656E-3	120.5804937E+0	117.2970265E+0
8	# M1	85.32831896E+0	7.695199592E-3	-6.000290809E+0	206.9107079E-3	221.2196752E-3	226.3788284E-3	237.4718544E-3	-56.11026564E+0	-56.39598110E+0	-24.10499184E+0	18.25038296E+0	132.7186366E+0	128.8594038E+0
8	# M1	85.32831896E+0	7.695199592E-3	-6.000290809E+0	206.9107079E-3	221.2196752E-3	226.3788284E-3	237.4718544E-3	-56.11026564E+0	-56.39598110E+0	-24.10499184E+0	18.25038296E+0	132.7186366E+0	128.8594038E+0
9	+ M1	9.470659212E+0	439.9960664E-3	-4.495931750E+0	180.4213420E-3	180.0000000E-3	183.7190468E-3	183.3039475E-3	27.69030396E+0	27.61999742E+0	-30.32211772E+0	19.35396965E+0	5.436109519E+0	5.447444121E+0

G.6.3 532 nm no crystal

#rs	label	ipp[mm]	rd[mm]	an2[deg]	w0t[mm]	w0s[mm]	w2t[mm]	w2s[mm]	z2t[mm]	z2s[mm]	x2[mm]	y2[mm]	Gp2t[deg]	Gp2s[deg]
1	+ M1	10.00009674E+0	-439.4599330E-3	5.247979444E+0	180.0000000E-3	180.0000000E-3	180.2456904E-3	180.2456904E-3	10.00009674E+0	10.00009674E+0	-30.40640984E+0	18.47856249E+0	1.495955217E+0	1.495955217E+0
2	# M1	9.459119252E+0	-16.8198788E-15	3.995931750E+0	180.4213420E-3	180.0000000E-3	180.9164800E-3	180.4953468E-3	21.37653115E+0	21.30622461E+0	-24.10418747E+0	18.25803601E+0	2.119975204E+0	2.122895745E+0
3	# M2	110.0469300E+0	-133.6301179E-3	-5.913924940E+0	79.91126239E-3	93.95099229E-3	139.2575817E-3	134.9773474E-3	53.81861719E+0	53.76762562E+0	85.91127409E+0	18.12513793E+0	55.56686931E+0	46.54200709E+0
4	# M3	87.80253813E+0	998.4401390E-6	5.912780812E+0	79.91126239E-3	93.95099229E-3	310.5678941E-3	271.9177637E-3	141.6211553E+0	141.5701638E+0	104.3753276E-6	-992.9695375E-6	65.62084892E+0	58.49094127E+0
5	+ PPKTP	24.40533251E+0	36.65299961E-3	-1.057399522E+0	16.19614588E-3	18.50996422E-3	57.30848271E-3	51.45613212E-3	-5.257670261E+0	-5.247954914E+0	24.40540786E+0	36.64567121E-3	72.33430240E+0	67.08091390E+0
6	# PPKTP	10.55146392E+0	-52.91845747E-3	88.36331631E-3	16.19614588E-3	18.50996422E-3	57.67087717E-3	51.93067557E-3	5.293793656E+0	5.303509003E+0	34.95685923E+0	52.91845747E-3	145.9710824E+0	136.0985744E+0
7	# M4	24.35955859E+0	-428.9751439E-3	6.087219188E+0	16.19614588E-3	18.50996422E-3	310.4671292E-3	272.0070314E-3	29.65335225E+0	29.66306759E+0	59.31638885E+0	90.48650430E-3	152.6310269E+0	144.5883306E+0
8	# M1	85.34363456E+0	299.8634542E-3	-6.086075060E+0	79.91126239E-3	93.95099229E-3	143.4695029E-3	138.2637202E-3	-56.22831282E+0	-56.27930439E+0	-24.13553174E+0	17.95981524E+0	162.0973792E+0	155.8877657E+0
8	# M1	85.34363456E+0	299.8634542E-3	-6.086075060E+0	79.91126239E-3	93.95099229E-3	143.4695029E-3	138.2637202E-3	-56.22831282E+0	-56.27930439E+0	-24.13553174E+0	17.95981524E+0	162.0973792E+0	155.8877657E+0
9	+ M1	9.470659212E+0	439.9960664E-3	-4.495931750E+0	180.4213420E-3	180.0000000E-3	181.2513932E-3	180.8316463E-3	27.69030396E+0	27.61999742E+0	-30.32211772E+0	19.35396965E+0	2.742743953E+0	2.748566949E+0

G.6.4 1064 nm no crystal

#rs	label	ipp[mm]	rd[mm]	an2[deg]	w0t[mm]	w0s[mm]	w2t[mm]	w2s[mm]	z2t[mm]	z2s[mm]	x2[mm]	y2[mm]	Gp2t[deg]	Gp2s[deg]
1	+ M1	10.00009674E+0	-439.4599330E-3	5.247979444E+0	180.0000000E-3	180.0000000E-3	180.9807602E-3	180.9807602E-3	10.00009674E+0	10.00009674E+0	-30.40640984E+0	18.47856249E+0	2.983796325E+0	2.983796325E+0
2	# M1	9.459119252E+0	-16.8198788E-15	3.995931750E+0	180.4213420E-3	180.0000000E-3	182.3938293E-3	181.9732970E-3	21.37653115E+0	21.30622461E+0	-24.10418747E+0	18.25803601E+0	4.216982801E+0	4.222729516E+0
3	# M2	110.0469300E+0	-133.6301179E-3	-5.913924940E+0	113.0115911E-3	132.8667675E-3	196.9399607E-3	190.8867953E-3	53.81861719E+0	53.76762562E+0	85.91127409E+0	18.12513793E+0	55.56686931E+0	46.54200709E+0
4	# M3	87.80253813E+0	998.4401396E-6	5.912780812E+0	113.0115911E-3	132.8667675E-3	439.2093279E-3	384.5497892E-3	141.6211553E+0	141.5701638E+0	104.3753277E-6	-992.9695380E-6	65.62084892E+0	58.49094127E+0
5	+ PPKTP	24.40533251E+0	36.65299961E-3	-1.057399522E+0	22.90480917E-3	26.17704244E-3	81.04643349E-3	72.76995992E-3	-5.257670261E+0	-5.247954914E+0	24.40540786E+0	36.64567121E-3	72.33430240E+0	67.08091390E+0
6	# PPKTP	10.55146392E+0	-52.91845747E-3	88.36331631E-3	22.90480917E-3	26.17704244E-3	81.55893665E-3	73.44106569E-3	5.293793656E+0	5.303509003E+0	34.95685923E+0	52.91845747E-3	145.9710824E+0	136.0985744E+0
7	# M4	24.35955859E+0	-428.9751439E-3	6.087219188E+0	22.90480917E-3	26.17704244E-3	439.0668248E-3	384.6760328E-3	29.65335225E+0	29.66306759E+0	59.31638885E+0	90.48650430E-3	152.6310269E+0	144.5883306E+0
8	# M1	85.34363456E+0	299.8634542E-3	-6.086075060E+0	113.0115911E-3	132.8667675E-3	202.8965168E-3	195.5344283E-3	-56.22831282E+0	-56.27930439E+0	-24.13553174E+0	17.95981524E+0	162.0973792E+0	155.8877657E+0
8	# M1	85.34363456E+0	299.8634542E-3	-6.086075060E+0	113.0115911E-3	132.8667675E-3	202.8965168E-3	195.5344283E-3	-56.22831282E+0	-56.27930439E+0	-24.13553174E+0	17.95981524E+0	162.0973792E+0	155.8877657E+0
9	+ M1	9.470659212E+0	439.9960664E-3	-4.495931750E+0	180.4213420E-3	180.0000000E-3	183.7190468E-3	183.3039475E-3	27.69030396E+0	27.61999742E+0	-30.32211772E+0	19.35396965E+0	5.436109519E+0	5.447444121E+0

G.6.5 532 nm with average crystal refractive index

#rs	label	ipp[mm]	rd[mm]	an2[deg]	w0t[mm]	w0s[mm]	w2t[mm]	w2s[mm]	z2t[mm]	z2s[mm]	x2[mm]	y2[mm]	Gp2t[deg]	Gp2s[deg]
1	+ M1	10.00009674E+0	-439.4599330E-3	5.247979444E+0	180.0000000E-3	180.0000000E-3	180.2456904E-3	180.2456904E-3	10.00009674E+0	10.00009674E+0	-30.40640984E+0	18.47856249E+0	1.495955217E+0	1.495955217E+0
2	# M1	9.459119252E+0	-16.8198788E-15	3.995931750E+0	180.4213420E-3	180.0000000E-3	180.9164800E-3	180.4953468E-3	21.37653115E+0	21.30622461E+0	-24.10418747E+0	18.25803601E+0	2.119975204E+0	2.122895745E+0
3	# M2	110.0014934E+0	8.88178420E-15	-6.000000000E+0	147.5581560E-3	157.8127836E-3	159.9966479E-3	167.9679268E-3	53.89476495E+0	53.60263384E+0	85.89730594E+0	18.25803601E+0	23.15818420E+0	20.50319761E+0
4	# M3	87.81630285E+0	63.1403191E-15	6.000000000E+0	147.5581560E-3	157.8127836E-3	219.5953714E-3	218.9355441E-3	141.7110678E+0	141.4189367E+0	6.59996053E-15	-62.7944298E-15	35.67833742E+0	32.42947218E+0
5	+ PPKTP	24.40614077E+0	-26.6453526E-15	-1.145762838E+0	21.11628884E-3	21.15926003E-3	31.11603735E-3	30.94793232E-3	-2.849837239E+0	-2.821950863E+0	24.40614077E+0	-25.3479348E-15	54.28764842E+0	51.22336667E+0
6	# PPKTP	19.62512052E+0	-97.56061696E-3	529.7887830E-3	21.11929114E-3	21.15926003E-3	30.95237382E-3	31.11645118E-3	5.248979631E+0	5.302355549E+0	34.95685923E+0	97.56061696E-3	101.4068597E+0	98.23452435E+0
7	# M4	24.40614077E+0	30.8257670E-15	6.492719464E+0	21.11707029E-3	21.15926003E-3	219.3607818E-3	219.1648447E-3	27.22758722E+0	27.25687752E+0	59.35939029E+0	517.3048927E-3	120.1571871E+0	116.8863138E+0
8	# M1	85.32820374E+0	-72.8306304E-15	-6.000000000E+0	147.5581560E-3	157.8127836E-3	160.9949912E-3	169.0189131E-3	-56.10672846E+0	-56.39885957E+0	-24.10418747E+0	18.25803601E+0	132.2329258E+0	128.3658983E+0
8	# M1	85.32820374E+0	-72.8306304E-15	-6.000000000E+0	147.5581560E-3	157.8127836E-3	160.9949912E-3	169.0189131E-3	-56.10672846E+0	-56.39885957E+0	-24.10418747E+0	18.25803601E+0	132.2329258E+0	128.3658983E+0
9	+ M1	9.470659212E+0	439.9960664E-3	-4.495931750E+0	180.4213420E-3	180.0000000E-3	181.2513932E-3	180.8316463E-3	27.69030396E+0	27.61999742E+0	-30.32211772E+0	19.35396965E+0	2.742743953E+0	2.748566949E+0

G.6.6 1064 nm with average crystal refractive index

#rs	label	ipp[mm]	rd[mm]	an2[deg]	w0t[mm]	w0s[mm]	w2t[mm]	w2s[mm]	z2t[mm]	z2s[mm]	x2[mm]	y2[mm]	Gp2t[deg]	Gp2s[deg]
1	+ M1	10.00009674E+0	-439.4599330E-3	5.247979444E+0	180.0000000E-3	180.0000000E-3	180.9807602E-3	180.9807602E-3	10.00009674E+0	10.00009674E+0	-30.40640984E+0	18.47856249E+0	2.983796325E+0	2.983796325E+0
2	# M1	9.459119252E+0	-16.8198788E-15	3.995931750E+0	180.4213420E-3	180.0000000E-3	182.3938293E-3	181.9732970E-3	21.37653115E+0	21.30622461E+0	-24.10418747E+0	18.25803601E+0	4.216982801E+0	4.222729516E+0
3	# M2	110.0014934E+0	8.88178420E-15	-6.000000000E+0	208.6787454E-3	223.1809789E-3	226.2694295E-3	237.5425202E-3	53.89476495E+0	53.60263384E+0	85.89730594E+0	18.25803601E+0	23.15818420E+0	20.50319761E+0
4	# M3	87.81630285E+0	63.1403191E-15	6.000000000E+0	208.6787454E-3	223.1809789E-3	310.5547524E-3	309.6216158E-3	141.7110678E+0	141.4189367E+0	6.59996053E-15	-62.7944298E-15	35.67833742E+0	32.42947218E+0
5	+ PPKTP	24.40614077E+0	-26.6453526E-15	-1.145762838E+0	29.86294206E-3	29.92371251E-3	44.00472203E-3	43.76698562E-3	-2.849837239E+0	-2.821950863E+0	24.40614077E+0	-25.3479348E-15	54.28764842E+0	51.22336667E+0
6	# PPKTP	19.62512052E+0	-97.56061696E-3	529.7887830E-3	29.86718796E-3	29.92371251E-3	43.77326684E-3	44.00530728E-3	5.248979631E+0	5.302355549E+0	34.95685923E+0	97.56061696E-3	101.4068597E+0	98.23452435E+0
7	# M4	24.40614077E+0	30.8257670E-15	6.492719464E+0	29.86404721E-3	29.92371251E-3	310.2229926E-3	309.9458958E-3	27.22758722E+0	27.25687752E+0	59.35939029E+0	517.3048927E-3	120.1571871E+0	116.8863138E+0
8	# M1	85.32820374E+0	-72.8306304E-15	-6.000000000E+0	208.6787454E-3	223.1809789E-3	227.6813001E-3	239.0288391E-3	-56.10672846E+0	-56.39885957E+0	-24.10418747E+0	18.25803601E+0	132.2329258E+0	128.3658983E+0
8	# M1	85.32820374E+0	-72.8306304E-15	-6.000000000E+0	208.6787454E-3	223.1809789E-3	227.6813001E-3	239.0288391E-3	-56.10672846E+0	-56.39885957E+0	-24.10418747E+0	18.25803601E+0	132.2329258E+0	128.3658983E+0
9	+ M1	9.470659212E+0	439.9960664E-3	-4.495931750E+0	180.4213420E-3	180.0000000E-3	183.7190468E-3	183.3039475E-3	27.69030396E+0	27.61999742E+0	-30.32211772E+0	19.35396965E+0	5.436109519E+0	5.447444121E+0

G.6.7 Box holes – normal direction

#rs	label	x1[mm]	y1[mm]	w1t[mm]	w1s[mm]	x2[mm]	y2[mm]	w2t[mm]	w2s[mm]
10	# Box right	89.02448615E+0	18.36746186E+0	227.4048622E-3	238.6450850E-3	131.2510000E+0	18.18129639E+0	262.4271934E-3	268.1201783E-3
12	# Box left	-5.869157082E+0	-1.034461060E+0	327.7736559E-3	326.1761616E-3	-71.94900000E+0	-15.08016527E+0	626.7094520E-3	612.1601132E-3
14	# Box right	65.32021826E+0	394.1130777E-3	367.2491986E-3	367.1205485E-3	131.2510000E+0	1.528178563E+0	1.321873303E+0	1.317408810E+0
16	# Box left	-30.32211772E+0	19.35396965E+0	183.0077429E-3	183.3039475E-3	-71.94900000E+0	28.39402996E+0	213.2544032E-3	213.4899312E-3

G.6.8 Box holes – reverse direction

#rs	label	x1[mm]	y1[mm]	w1t[mm]	w1s[mm]	x2[mm]	y2[mm]	w2t[mm]	w2s[mm]
10	# Box right	65.23394866E+0	-500.6392548E-3	327.4447523E-3	326.5326400E-3	131.2510000E+0	-14.53299670E+0	626.3400714E-3	612.6574749E-3
12	# Box left	-5.955978466E+0	-208.4107683E-3	367.6013550E-3	366.7514778E-3	-71.94900000E+0	-208.4107683E-3	1.322716743E+0	1.317451605E+0
14	# Box right	88.97514576E+0	18.80051688E+0	225.1538558E-3	236.4784702E-3	131.2510000E+0	27.59235184E+0	209.3074280E-3	223.5394339E-3
16	# Box left	-30.40640984E+0	18.47856249E+0	222.1940568E-3	221.8648137E-3	-71.94900000E+0	18.66129243E+0	238.9697450E-3	238.7168332E-3

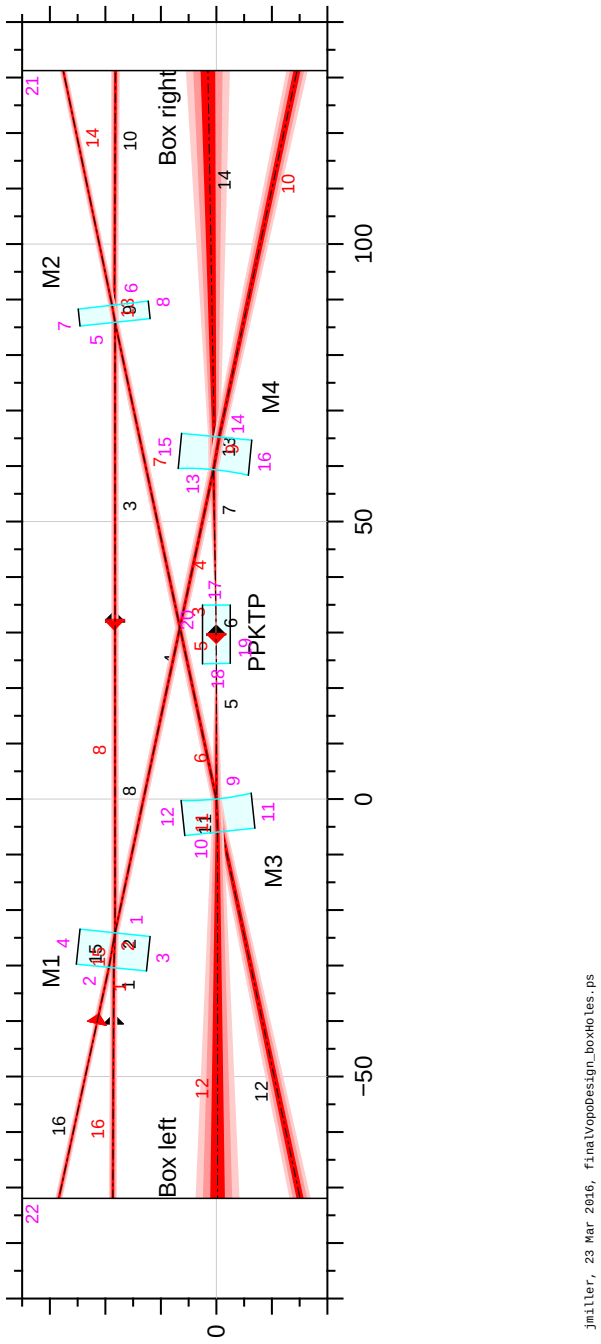

Figure 19: OptoCad model of the VOPO, in this instance for 1064 nm fields entering in two directions. Black numbers correspond to the ray segment labels used section G.6.7; red labels correspond to section G.6.8.

H Old designs

In this section we detail the properties of previous OPO designs so that the latest VOPO may be better judged by comparison.

H.1 H1 OPO

Here we refer to the cavity used for the H1 experiment and past in-air tests at MIT and The ANU. The cavity from the era of Sheila Dwyer et al.

To the best of my knowledge there is no document describing the design of the H1 OPO. The best source is [2]; however, this thesis omits some useful quantities and has an error in its ABCD matrix calculations. Here we attempt to give a more complete description of our 'standard' OPO.

The parameters of the H1 OPO are listed in Table 10. Here and elsewhere in this document one should assume that given values are of the nominal design rather than measured as-built numbers. All dimensions presented are physical, as opposed to optical, lengths.

The transverse mode spectra for 532 nm and 1064 nm are shown in Figure 20.

Beam spot sizes as a function of propagation distance from M1 are shown in Figure 21.

H.1.1 Discussion

As far as I am aware the H1 OPO was (and would be) adequate. The decision to change geometry for VOPO1 was made in order to mitigate clipping of the diagonal beams on the tombstones of M3 and M4. This issue is depicted in Figure 22.

In the unrealistic limit of perfect alignment, beam clipping is not an issue. Furthermore, if we assume that the level of beam clipping caused by the mirror itself is acceptable (the H1 VOPO suffered from such clipping) the issue may be easily mitigated by reducing the width of the tombstones by 1.5-2 mm on one side. This is eminently feasible given the current half-width of the tombstone (10 mm), radii of the PZT (7.5 mm) and radii of the mirrors (6.35 mm). A smaller PZT (e.g. the Noliac NAC2123 with a radius of 6 mm) could be used if necessary. Smaller diameter mirrors are not stock items from our current vendor (Laseroptik).

Another simple way to avoid clipping issues is to increase the angle of incidence on the optics from 6 to 7 degrees. This approach is less desirable as it increases the astigmatism of the cavity, albeit by a small amount.

The H1 OPO does have a somewhat low g factor but there is no evidence that this has hampered performance in any way. The same can be said of the fact that the fifth order modes overlap with the fundamental.

Table 10: Parameters of the H1 OPO. The cavity lengths are derived from the flat mirror separation and total round-trip optical length given in [2], assuming that the optical path was calculated for 1064 nm. Sagittal and tangential planes are denoted by (s) and (t) respectively. The calculation of alignment sensitivity is described in section G.4.

Parameter	Value	
flatSep	90.000 mm	
curveSep	43.628 mm	
flatCurveSep	68.307 mm	
ROC	38.0 mm	
θ_{aoi}	6.0°	
	532 nm	1064 nm
Finesse, crystal in	16.8	42.5
Linewidth, crystal in	63.707 MHz	25.289 MHz
FSR, crystal in	1072.110 MHz	1074.514 MHz
$\omega_0^{\mathrm{small}}$, crystal in	12.4 µm (s)/14.3 µm (t)	19.0 µm (s)/21.0 µm (t)
$\omega_0^{\mathrm{large}}$, crystal in	253.2 µm (s)/210.6 µm (t)	327.1 µm (s)/282.2 µm (t)
g factor, crystal in	0.058 (s)/ 0.115 (t)	0.082 (s)/ 0.139 (t)
Gouy phase, crystal in	0.578π (s)/0.610π (t)	0.592π (s)/0.622π (t)
Alignment sensitivity, crystal in	0.140 m/rad (s)/ 0.150 m/rad (t)	0.144 m/rad (s)/ 0.154 m/rad (t)
Relative alignment sensitivity, crystal in	0.553 $\omega_0^{\mathrm{large}}$/mrad (s)/ 0.711 $\omega_0^{\mathrm{large}}$/mrad (t)	0.439 $\omega_0^{\mathrm{large}}$/mrad (s)/ 0.546 $\omega_0^{\mathrm{large}}$/mrad (t)
FSR, crystal out	1109.348 MHz	
$\omega_0^{\mathrm{small}}$, crystal out	17.3 µm (s)/16.4 µm (t)	24.5 µm (s)/23.2 µm (t)
$\omega_0^{\mathrm{large}}$, crystal out	102.3 µm (s)/93.3 µm (t)	144.6 µm (s)/131.9 µm (t)
g factor, crystal out	0.699 (s)/ 0.772 (t)	
Gouy phase, crystal out	0.815π (s)/0.841π (t)	
Alignment sensitivity, crystal out	0.447 m/rad (s)/0.592 m/rad (t)	
Relative alignment sensitivity, crystal out	4.370 $\omega_0^{\mathrm{large}}$/mrad (s)/ 6.344 $\omega_0^{\mathrm{large}}$/mrad (t)	3.090 $\omega_0^{\mathrm{large}}$/mrad (s)/ 4.486 $\omega_0^{\mathrm{large}}$/mrad (t)

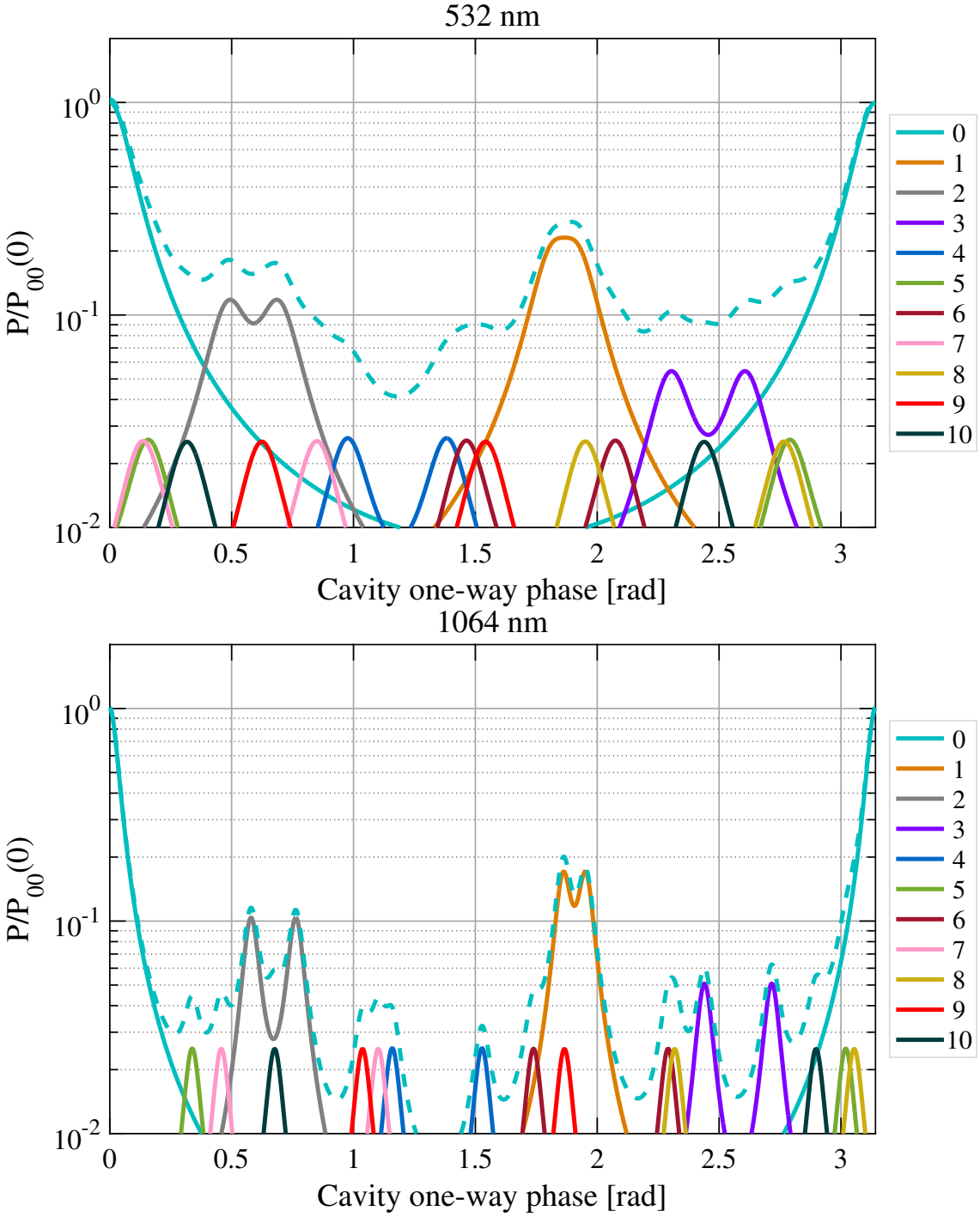

Figure 20: Simulated transverse mode spectrum of the H1 OPO. Legend values indicate mode order. For each order, peaks are only drawn for the highest and lowest frequency modes (e.g. 20 and 02 but not 11). The relative powers in each mode were chosen arbitrarily. The total power is given by the dashed trace.

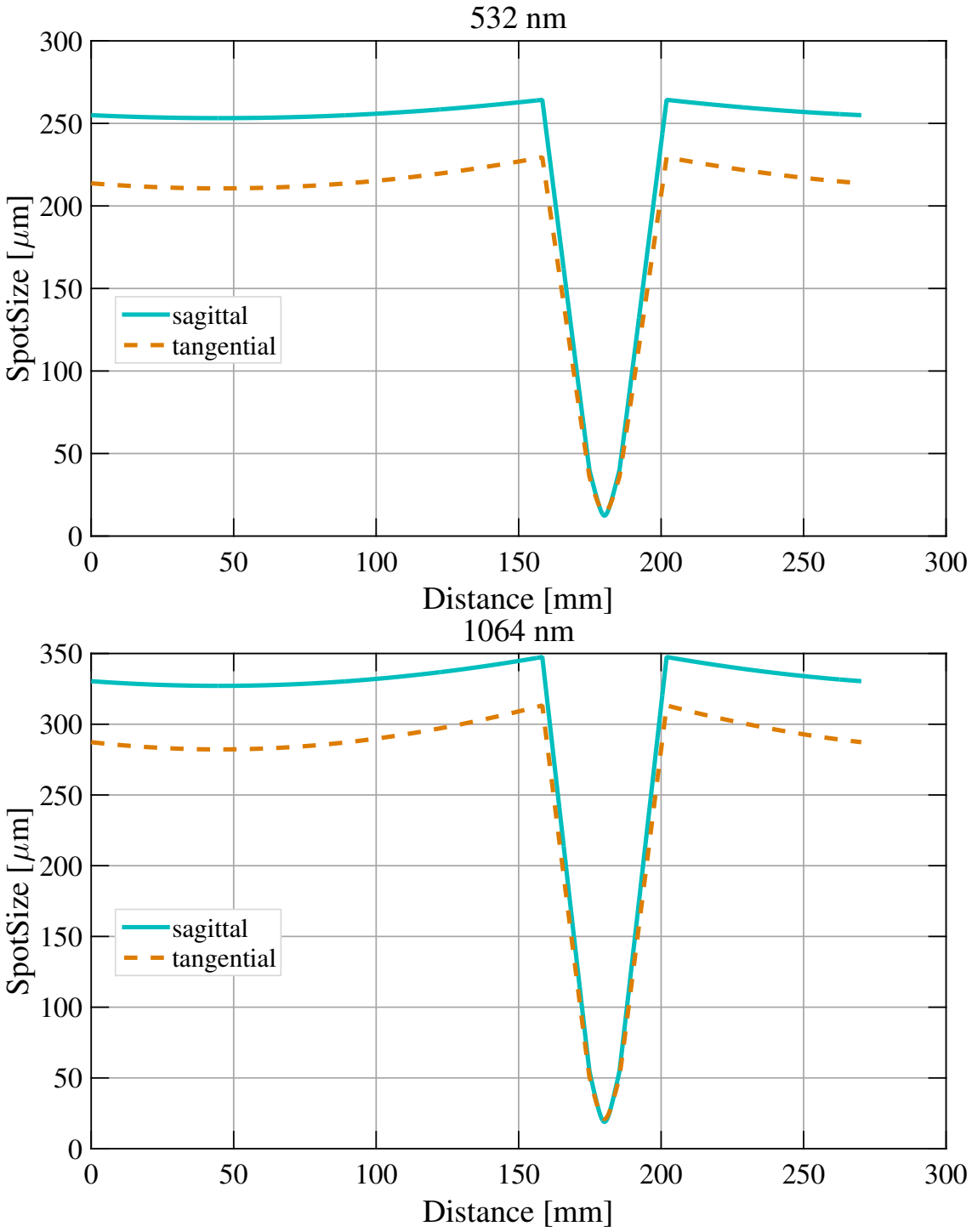

Figure 21: Beam spot size as a function of distance from M1 for the H1 OPO.

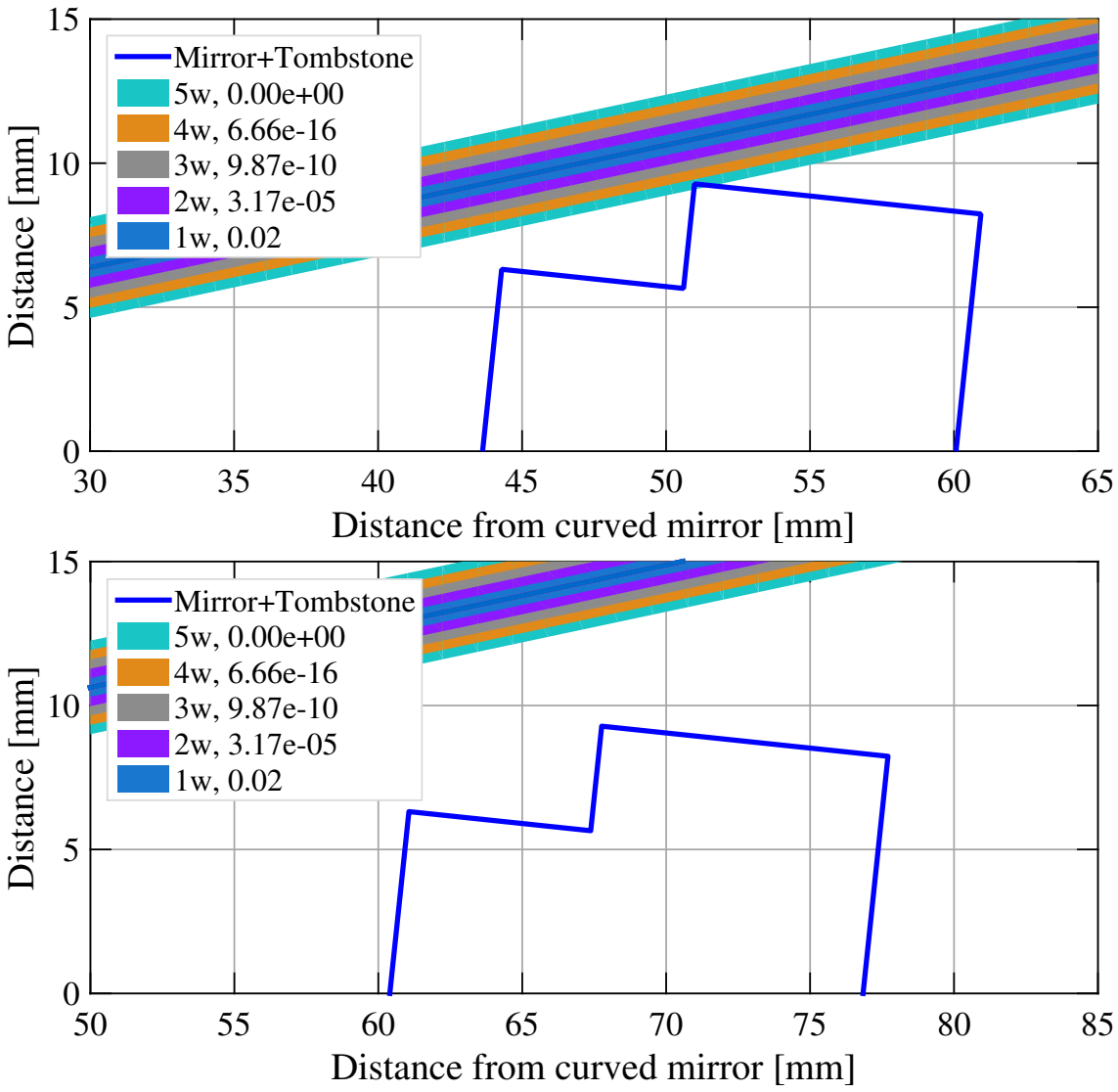

Figure 22: Beam clipping on the tombstones. Upper: H1 OPO, Lower: VOPO1. Plots show the outline of M4 and its tombstone in blue along with the axis of the beam heading from M2 to M3. Contours indicate the width of the beam in units of beam spot size with the values in the legend indicating the corresponding power loss should the beam be clipped on one side to that level. For example, the power loss associated with beam clipping in the upper plot is $\lesssim 6.7 \times 10^{-16}$.

H.2 VOPO1

The first generation of in-vacuum cavity built using tombstones on a glass substrate, the kind constructed by Georgia Mansell and Andrew Wade.

The design parameters of VOPO1 are given in Table 11

Table 11: Parameters of VOPO1. Sagittal and tangential planes are denoted by (s) and (t) respectively. The calculation of alignment sensitivity is described in section G.4.

Parameter	Value	
flatSep	110.000 mm	
curveSep	60.400 mm	
flatCurveSep	87.103 mm	
ROC	50.0 mm	
θ_{aoi}	6.0°	
	532 nm	1064 nm
Finesse, crystal in	16.8	35.3
Linewidth, crystal in	50.324 MHz	24.062 MHz
FSR, crystal in	846.888 MHz	848.387 MHz
$\omega_0^{\mathrm{small}}$, crystal in	21.4 µm (s)/21.1 µm (t)	30.2 µm (s)/29.8 µm (t)
$\omega_0^{\mathrm{large}}$, crystal in	144.0 µm (s)/135.2 µm (t)	200.2 µm (s)/187.9 µm (t)
g factor, crystal in	0.477 (s)/ 0.541 (t)	0.494 (s)/ 0.558 (t)
Gouy phase, crystal in	0.743π (s)/0.763π (t)	0.748π (s)/0.769π (t)
Alignment sensitivity, crystal in	0.323 m/rad (s)/ 0.370 m/rad (t)	0.334 m/rad (s)/ 0.385 m/rad (t)
Relative alignment sensitivity, crystal in	2.244 $\omega_0^{\mathrm{large}}$/mrad (s)/ 2.737 $\omega_0^{\mathrm{large}}$/mrad (t)	1.668 $\omega_0^{\mathrm{large}}$/mrad (s)/ 2.047 $\omega_0^{\mathrm{large}}$/mrad (t)
FSR, crystal out	869.955 MHz	
$\omega_0^{\mathrm{small}}$, crystal out	14.9 µm (s)/0.0 µm (t)	21.1 µm (s)/0.0 µm (t)
$\omega_0^{\mathrm{large}}$, crystal out	71.7 µm (s)/0.0 µm (t)	101.3 µm (s)/0.0 µm (t)
g factor, crystal out	0.937 (s)/ 1.012 (t)	
Gouy phase, crystal out	0.919π (s)/NaNπ (t)	
Alignment sensitivity, crystal out	2.721 m/rad (s)/NaN m/rad (t)	
Relative alignment sensitivity, crystal out	37.979 $\omega_0^{\mathrm{large}}$/mrad (s)/ NaN $\omega_0^{\mathrm{large}}$/mrad (t)	26.855 $\omega_0^{\mathrm{large}}$/mrad (s)/ NaN $\omega_0^{\mathrm{large}}$/mrad (t)

The transverse mode spectra for 532 nm and 1064 nm are shown in Figure 25.

Beam spot sizes as a function of propagation distance from M1 are shown in Figure 26.

H.2.1 Discussion

The cavity geometry employed in VOPO1 has not been tested as extensively as the H1 OPO's. Initial results report less squeezing and larger phase noise but these measurements are likely not indicative of possible performance.

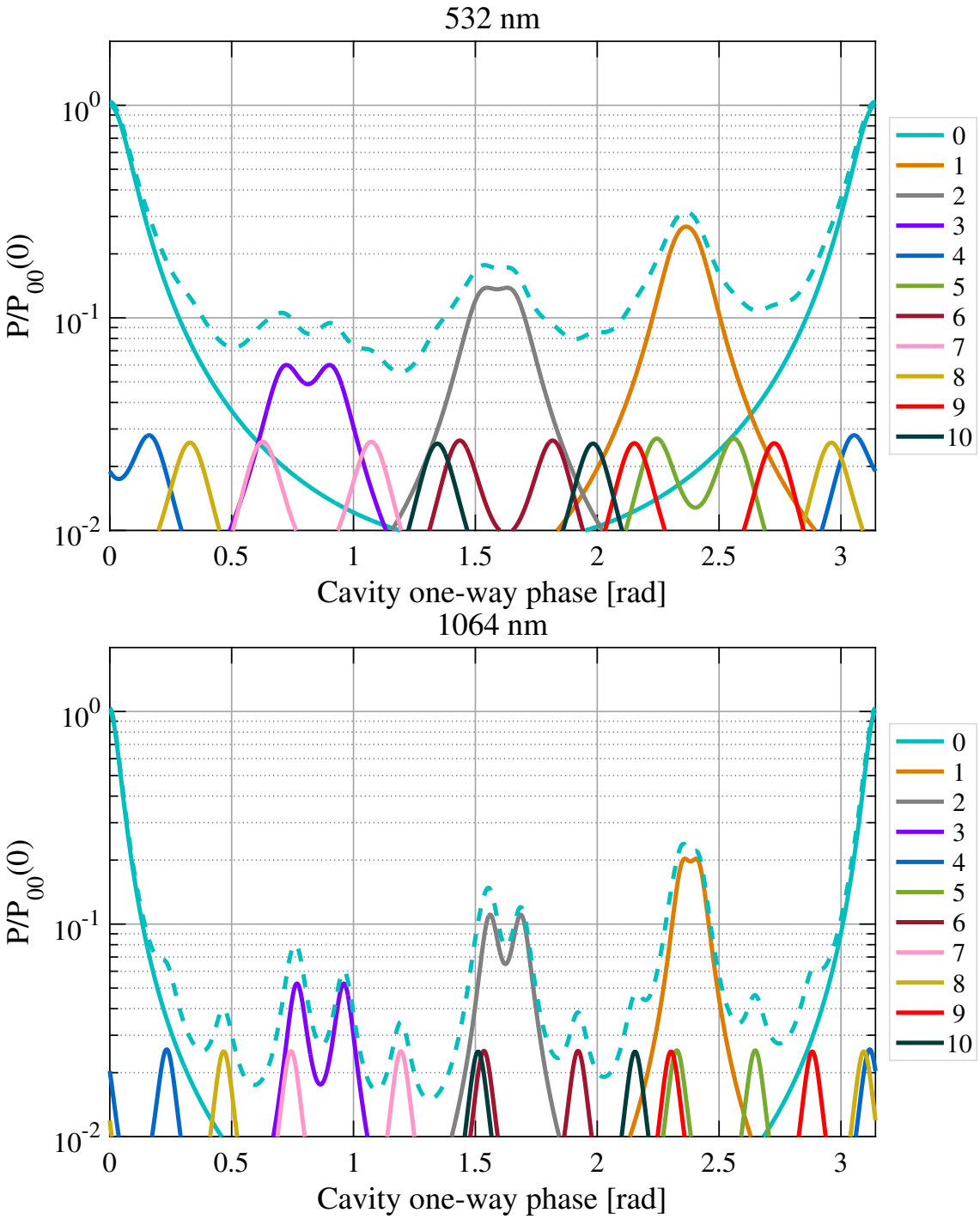

Figure 23: Simulated transverse mode spectrum of VOPO1. Legend values indicate mode order. For each order, peaks are only drawn for the highest and lowest frequency modes (e.g. 20 and 02 but not 11). The relative powers in each mode were chosen arbitrarily. The total power is given by the dashed trace.

The cavity is unstable in the tangential plane when the crystal is removed. Stability with no crystal is important as, measurements of loss in this configuration can be useful in charac-

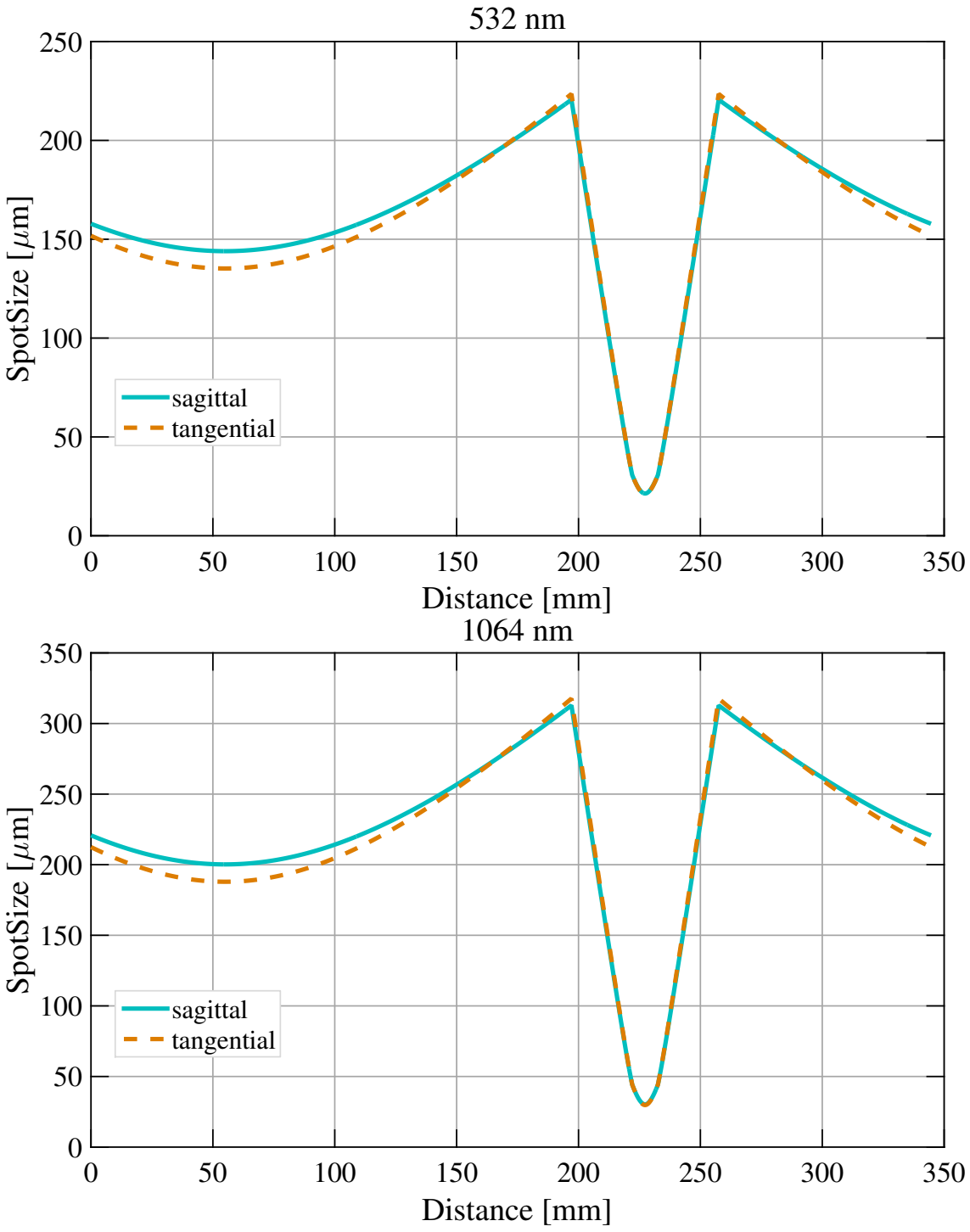

Figure 24: Beam spot size as a function of distance from M1 for VOPO1.

terising the cavity. However, the spot sizes on the mirrors change somewhat when removing the crystal so care must be taken in interpreting the results of such measurements.

The beam waist size inside the crystal is larger in VOPO1 with respect to the H1 OPO. VOPO1 has a ξ (see section F) of approximately 1. This change should have a very modest

impact on attainable squeezing levels and may help with thermal effects.

Fourth order modes overlap with the fundamental in the VOPO1 design. Given the low finesse, particularly for 532 nm, it is difficult to avoid such overlaps but small changes in the lengths can yield improvements.

The cavity mode spacing is also very sensitive to the separation of the curved mirrors. For example, changing the separation of the curved mirrors by ∼0.5 mm will make the third rather than the fourth order modes overlap with the fundamental.

H.3 VOPO2 sans wedge

The initial design of VOPO2 was conducted ignoring the wedge on the PPKTP crystal. This design is detailed here so that one can gauge the effect of including this wedge. It is negligible.

The design parameters of wedgeless VOPO2 are given in Table 12

The transverse mode spectra for 532 nm and 1064 nm are shown in Figure 25.

Beam spot sizes as a function of propagation distance from M1 are shown in Figure 26.

Table 12: Parameters of the wedgeless VOPO2 cavity. Sagittal and tangential planes are denoted by (s) and (t) respectively. The calculation of alignment sensitivity is described in section G.4.

Parameter	Value	
flatSep	110.000 mm	
curveSep	59.363 mm	
flatCurveSep	86.573 mm	
ROC	50.0 mm	
θ_{aoi}	6.0°	
	532 nm	1064 nm
Finesse, crystal in	34.8	46.1
Linewidth, crystal in	24.499 MHz	18.495 MHz
FSR, crystal in	851.934 MHz	853.451 MHz
ω_0^{small}, crystal in	21.1 µm (s)/21.1 µm (t)	30.0 µm (s)/29.9 µm (t)
ω_0^{large}, crystal in	158.8 µm (s)/149.2 µm (t)	220.6 µm (s)/207.4 µm (t)
g factor, crystal in	0.380 (s)/ 0.441 (t)	0.396 (s)/ 0.458 (t)
Gouy phase, crystal in	0.711π (s)/0.731π (t)	0.717π (s)/0.737π (t)
Alignment sensitivity, crystal in	0.271 m/rad (s)/ 0.302 m/rad (t)	0.278 m/rad (s)/ 0.311 m/rad (t)
Relative alignment sensitivity, crystal in	1.704 ω_0^{large}/mrad (s)/ 2.023 ω_0^{large}/mrad (t)	1.261 ω_0^{large}/mrad (s)/ 1.502 ω_0^{large}/mrad (t)
FSR, crystal out	875.281 MHz	
ω_0^{small}, crystal out	18.4 µm (s)/16.0 µm (t)	26.0 µm (s)/22.7 µm (t)
ω_0^{large}, crystal out	93.2 µm (s)/78.9 µm (t)	131.9 µm (s)/111.6 µm (t)
g factor, crystal out	0.837 (s)/ 0.910 (t)	
Gouy phase, crystal out	0.868π (s)/0.903π (t)	
Alignment sensitivity, crystal out	1.047 m/rad (s)/1.897 m/rad (t)	
Relative alignment sensitivity, crystal out	11.225 ω_0^{large}/mrad (s)/ 24.046 ω_0^{large}/mrad (t)	7.937 ω_0^{large}/mrad (s)/ 17.003 ω_0^{large}/mrad (t)

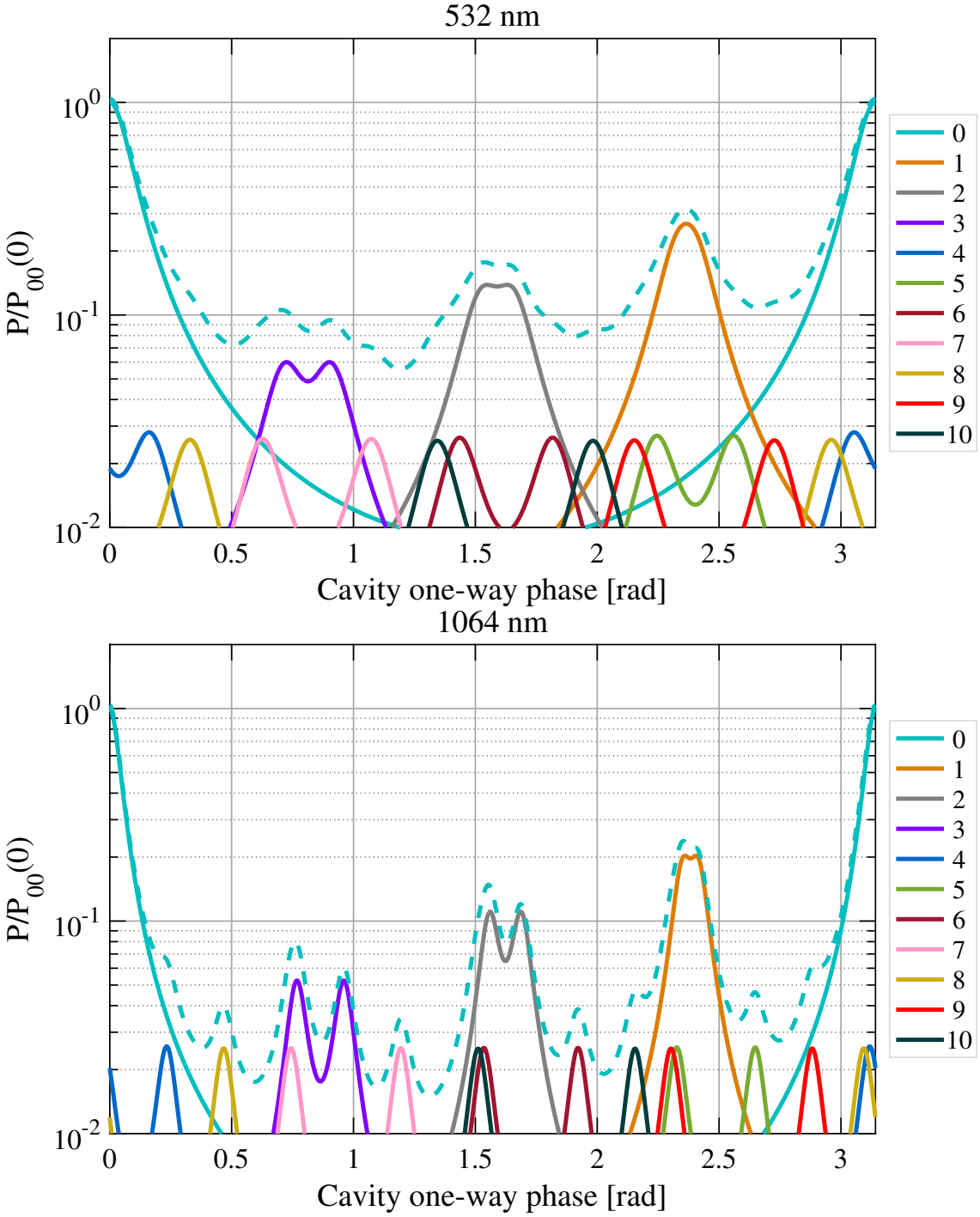

Figure 25: Simulated transverse mode spectrum of VOPO1. Legend values indicate mode order. For each order, peaks are only drawn for the highest and lowest frequency modes (e.g. 20 and 02 but not 11). The relative powers in each mode were chosen arbitrarily. The total power is given by the dashed trace.

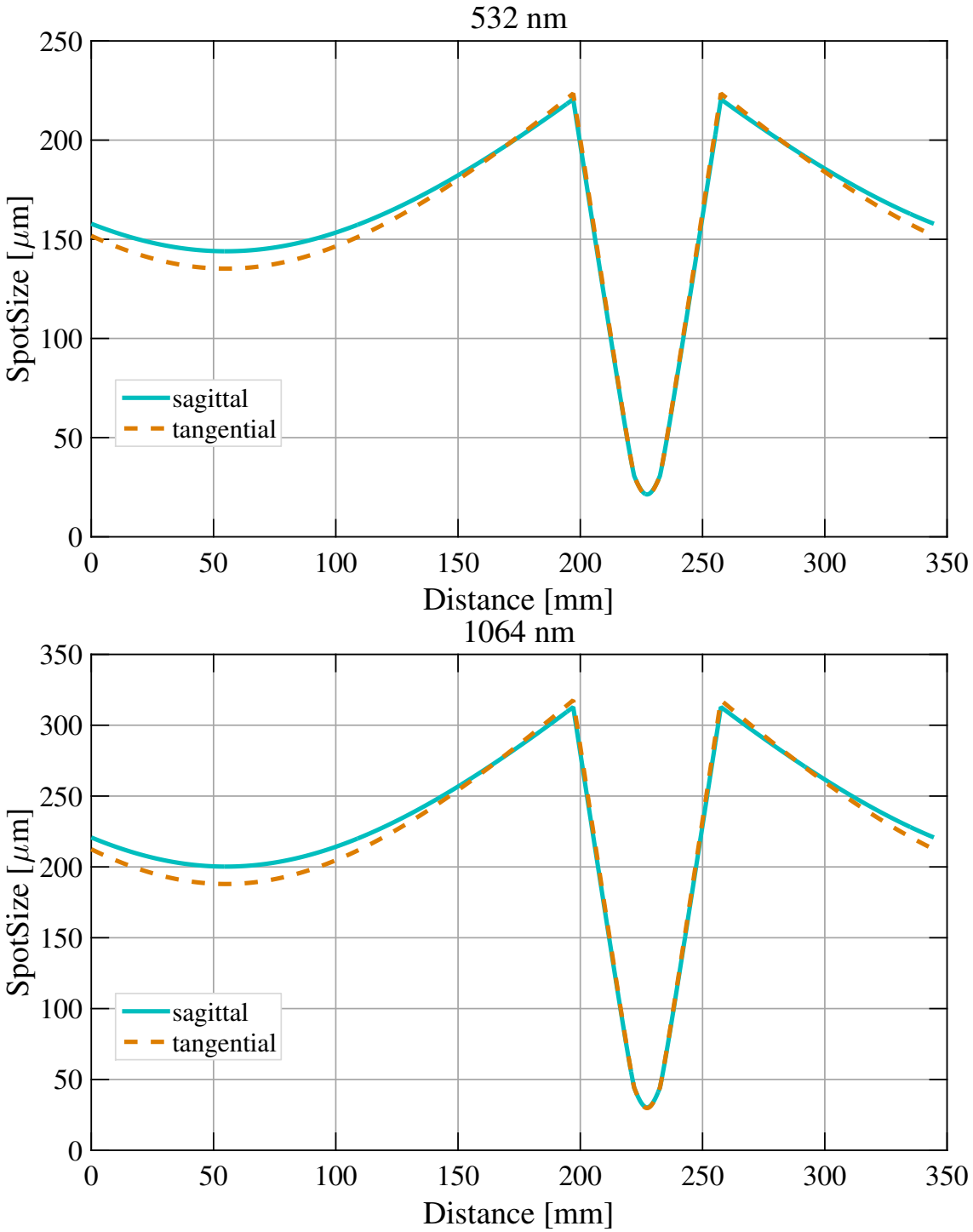

Figure 26: Beam spot size as a function of distance from M1 for VOPO1.

References

[1] S. S. Y. Chua, M. S. Stefszky, C. M. Mow-Lowry, B. C. Buchler, S. Dwyer, D. A. Shaddock, P. K. Lam, and D. E. McClelland, "Backscatter tolerant squeezed light source for advanced gravitational-wave detectors," *Optics Letters*, vol. 36, p. 4680, Dec. 2011.

[2] M. Stefszky, *Generation and Detection of Low-Frequency Squeezing for Gravitational-Wave Detection*. PhD thesis, The Australian National University, 2012.

[3] https://dcc.ligo.org/DocDB/0012/C1000923/001/C1000923-v1.pdf.

[4] https://maz.mit.edu/sqwiki/H1SqueezerCrystals.

[5] S. Dwyer, *Quantum noise reduction using squeezed states in LIGO*. PhD thesis, Massachusetts Institute of Technology, 2013.

[6] P. Kwee, J. Miller, T. Isogai, L. Barsotti, and M. Evans, "Decoherence and degradation of squeezed states in quantum filter cavities," *Phys. Rev. D*, vol. 90, p. 062006, Sep 2014.

[7] S. Dwyer, L. Barsotti, S. S. Y. Chua, M. Evans, M. Factourovich, D. Gustafson, T. Isogai, K. Kawabe, A. Khalaidovski, P. K. Lam, M. Landry, N. Mavalvala, D. E. McClelland, G. D. Meadors, C. M. Mow-Lowry, R. Schnabel, R. M. S. Schofield, N. Smith-Lefebvre, M. Stefszky, C. Vorvick, and D. Sigg, "Squeezed quadrature fluctuations in a gravitational wave detector using squeezed light," *Optics Express*, vol. 21, p. 19047, Aug. 2013.

[8] "H1 OMC cavity length noise measurement with PDH locking." eLog, Jan. 2015. https://alog.ligo-wa.caltech.edu/aLOG/index.php?callRep=16089.

[9] E. Oelker, L. Barsotti, S. Dwyer, D. Sigg, and N. Mavalvala, "Squeezed light for advanced gravitational wave detectors and beyond," *Optics Express*, vol. 22, p. 21106, Aug. 2014.

[10] M. E. Innocenzi, H. T. Yura, C. L. Fincher, and R. A. Fields, "Thermal modeling of continuouswave endpumped solidstate lasers," *Applied Physics Letters*, vol. 56, no. 19, pp. 1831–1833, 1990.

[11] A. Douillet, J.-J. Zondy, A. Yelisseyev, S. Lobanov, and L. Isaenko, "Stability and frequency tuning of thermally loaded continuous-wave aggas2 optical parametric oscillators," *J. Opt. Soc. Am. B*, vol. 16, pp. 1481–1498, Sep 1999.

[12] H. Rabin, *Quantum electronics : a treatise*. New York: Academic Press, 1975.

[13] G. D. Boyd and D. A. Kleinman, "Parametric interaction of focused gaussian light beams," *Journal of Applied Physics*, vol. 39, no. 8, pp. 3597–3639, 1968.

[14] R. Schilling, "OptoCad version 0.94a." OptoCad webpage. http://home.rzg.mpg.de/ ros/optocad.html.

[15] G. A. Massey and A. E. Siegman, "Reflection and refraction of gaussian light beams at tilted ellipsoidal surfaces," *Appl. Opt.*, vol. 8, pp. 975–978, May 1969.

[16] K. Arai, "On the accumulated round-trip gouy phase shift for a general optical cavity angular stability in a triangular fabry-perot cavity," tech. rep., LIGO Laboratory, 2013. https://dcc.ligo.org/LIGO-T1300189.

[17] A. Gerrard and J. Burch, *Introduction to matrix methods in optics.* p286, New York: Dover, 1994.

[18] H. Carstens, S. Holzberger, J. Kaster, J. Weitenberg, V. Pervak, A. Apolonski, E. Fill, F. Krausz, and I. Pupeza, "Large-mode enhancement cavities," *Opt. Express*, vol. 21, pp. 11606–11617, May 2013.

[19] V. Magni, "Multielement stable resonators containing a variable lens," *Journal of the Optical Society of America A*, vol. 4, pp. 1962–1969, Oct. 1987.

[20] A. A. Tovar and L. W. Casperson, "Generalized beam matrices: Gaussian beam propagation in misaligned complex optical systems," *Journal of the Optical Society of America A*, vol. 12, pp. 1522–1533, July 1995.

[21] W. J. Firth and A. M. Yao, "Master equation for misaligned cavities," *Journal of Modern Optics*, vol. 53, pp. 2005–2010, 2006.

[22] S. Waldman, "Ray optics calculations of alignment matrices," Tech. Rep. LIGO-T0900647-v2, LIGO Laboratory, 2009.

[23] D. Sigg, "Angular Instabilities in High Power Fabry-Perot Cavities," Tech. Rep. LIGO-T030120-x0, LIGO Laboratory, 2003.

[24] A. E. Siegman, *Lasers.* p591, University Science Books, 1986.